Comparison of Steric and Electronic Requirements for C−C and C−H Bond Activation. Chelating vs Nonchelating Case

Boris Rybtchinski,[†] Stephan Oevers,[†] Michael Montag,[†] Arkadi Vigalok,[†] Haim Rozenberg,[‡] Jan M. L. Martin,*[,†] and David Milstein*[,†]

Contribution from the Department of Organic Chemistry and Chemical Services Unit, Weizmann Institute of Science, 76100 Rehovot, Israel

Received May 2, 2001

Abstract: C−H bond activation was observed in a novel PCO ligand **1** ($C_6H(CH_3)_3(CH_2OCH_3)(CH_2P(t\text{-}Bu)_2)$) at room temperature in THF, acetone, and methanol upon reaction with the cationic rhodium precursor, $[Rh(coe)_2(solv)_n]BF_4$ (solv = solvent; coe = cyclooctene). The products in acetone (complexes **3a** and **3b**) and methanol (complexes **4a** and **4b**) were fully characterized spectroscopically. Two products were formed in each case, namely those containing uncoordinated (**3a** and **4a**) and coordinated (**3b** and **4b**) methoxy arms, respectively. Upon heating of the C−H activation products in methanol at 70 °C, C−C bond activation takes place. Solvent evaporation under vacuum at room temperature for 3−4 days also results in C−C activation. The C−C activation product, $((CH_3)Rh(C_6H(CH_3)_2(CH_2OCH_3)(CH_2P(t\text{-}Bu)_2)BF_4)$, was characterized by X-ray crystallography, which revealed a square pyramidal geometry with the BF_4^- anion coordinated to the metal. Comparison to the structurally similar and isoelectronic nonchelating Rh−PC complex system and computational studies provide insight into the reaction mechanism. The reaction mechanism was studied computationally by means of a two-layer ONIOM model, using both the B3LYP and mPW1K exchange-correlation functionals and a variety of basis sets. Polarization functions significantly affect relative energetics, and the mPW1K profile appears to be more reliable than its B3LYP counterpart. The calculations reveal that the electronic requirements for both C−C and C−H activation are essentially the same (14e intermediates are the key ones). On the other hand, the steric requirements differ significantly, and chelation appears to play an important role in C−C bond activation.

Introduction

Carbon−carbon and carbon−hydrogen bond activation by transition metal complexes are topics of much current interest. Metal-promoted activation of C−C and C−H bonds in homogeneous media under mild conditions may lead to the design of new selective processes for the utilization of hydrocarbons.[1,2] Many examples of both intra- and intermolecular C−H bond activation are known, and mechanistic studies of these processes have revealed that agostic intermediates and σ-alkane complexes can be involved.[2] Coordinative unsaturation is an important requirement for C−H bond cleavage.[3] Theoretical calculations are in line with these findings and provide further insight into the details of the reaction mechanism.[4]

Examples of carbon−carbon bond activation in solution are scarce relative to those of carbon−hydrogen bond activation, since, in general, kinetic and thermodynamic factors favor C−H over C−C activation. Since C−H bonds are generally more accessible sterically than C−C bonds, activation of the former is normally kinetically more favorable. The higher degree of C−C bond directionality (sp^3-sp^3) compared to that of C−H (sp^3-s) was also suggested to significantly contribute to the higher kinetic barriers for C−C bond activation.[5] An additional thermodynamic driving force, such as strain relief or aromatization, is generally required for C−C activation to take place.[1] Nonetheless, it is possible to design a C−C activation system in such a way that the reaction is driven by formation of strong bonds and/or volatile products (such as CH_4 or C_2H_4). We have demonstrated that the PCP (i.e., symmetric chelated system with two phosphine arms) and PCN (i.e., asymmetric chelated system with one amino and one phosphino arm) ligand systems are extremely efficient in the activation of strong, unstrained, nonactivated C−C bonds, which are situated between the two chelating arms of the ligand.[6,7] Theoretical calculations,[8] and a kinetic study of a direct, single-step insertion of a neutral Rh(I) complex into a strong C−C bond,[9] reveal that the reaction mechanism involves a nonpolar three-centered transition state. Understanding the factors which control C−C vs C−H activation is of prime importance. Here we report on an experimental and theoretical study of competitive carbon−carbon and carbon−hydrogen bond activation processes in a novel PCO (i.e., asymmetric chelated system with one phosphine and one

* To whom correspondence should be addressed. E-mail: comartin@wicc.weizmann.ac.il, david.milstein@weizmann.ac.il.

[†] Department of Organic Chemistry.

[‡] Chemical Services Unit.

(1) For recent reviews on C−C bond activation, see: (a) Rybtchinski, B.; Milstein, D. *Angew. Chem., Int. Ed.* **1999**, 38, 870. (b) Murakami, M.; Ito, Y. In *Topics in Organometallic Chemistry*; Murai, S., Ed.; Springer-Verlag: Berlin Heidelberg, 1999; Vol. 3, p 97.

(2) (a) Hall, C.; Perutz, R. N. *Chem. Rev.* **1996**, *96*, 3125, (b) Shilov, A. E.; Shul'pin, G. B. *Chem. Rev.* **1997**, *97*, 2879.

(3) Milstein, D. *Acc. Chem. Res.* **1984**, *17*, 221.

(4) For the review see: Niu, S.; Hall, M. B. *Chem. Rev.* **2000**, *100*, 353. See also: Saillard, J.-Y.; Hoffman R. *J. Am. Chem. Soc.* **1984**, *106*, 2006.

(5) (a) Low J. J.; Goddard, W. A., III. *J. Am. Chem. Soc.* **1984**, *106*, 10779. (b) Blomberg, M. R. A.; Siegbahn, P. E. M.; Nagashima, U.; Wennerberg, J. *J. Am. Chem. Soc.* **1991**, *113*, 424. (c) Siegbahn, P. E. M. Blomberg, M. R. A. *J. Am. Chem. Soc.* **1992**, *114*, 10548.

10.1021/ja016126t CCC: $20.00
Published on Web 08/25/2001

methoxy arm) ligand system involving a cationic Rh(I) complex. Our studies clearly show that the methoxy moiety, although being a relatively weak ligand, plays a critical role in the C−C bond activation process: this demonstrates that chelation of the methoxy group to the metal center is fundamental to the chemistry of C−C activation in this system. Coordinated solvent molecules also play an important role in the activation processes. Remarkably, we show that the reaction can be controlled not only by the coordinating ability of the solvent, but merely *by the presence or absence of the solvent in the reaction*. In the presence of a coordinating solvent (methanol) only C−H bond activation takes place, while C−C bond activation can be selectively achieved simply by solvent evaporation. Theoretical calculations have provided important insight into the reaction mechanism. It was found that cationic 14-electron Rh(I) complexes are key intermediates in both C−H and C−C activation and that the chelating effect facilitates C−C activation both kinetically and thermodynamically. A comparison of the transition states for C−C and C−H activation indicates that specific steric requirements are important for achieving metal insertion into the C−C bond. Another important finding is that coordination of solvent molecules (methanol or ether) to a cationic Rh(I) metal center can significantly lower the kinetic barrier of C−H as well as C−C activation.

Experimental Results

Ligand Design and Synthesis. In our quest for a better understanding of the factors which are important for C−C bond activation, we planned to study the significance of the chelating effect. The novel PCO-type ligand **1** was designed to create a C−C activating system in which one of the chelating moieties is labile. The mono-chelating PC system studied by us appeared to be inactive in C−C bond activation.[10] The PCO ligand system mimics the electron density environment and general structure of the mono-chelating PC system, but it potentially enables both mono- and bis-chelating binding modes. Thus, the PCO ligand system may reveal the impact of the chelate effect as a controlling factor in C−C vs C−H bond activation.

Ligand **1**, 1-methoxymethyl-3-(di-*tert*-butylphosphino)methyl-2,4,6-trimethylbenzene, was synthesized (Scheme 1) from 1,3-bis(bromomethyl)-2,4,6-trimethylbenzene, which was prepared according to a literature procedure.[11] Reaction of the dibromide with NaOMe produced the mono-methoxy intermediate, 1-bromomethyl-3-methoxymethyl-2,4,6-trimethylbenzene. This compound was then reacted with di-*tert*-butylphosphine to yield the corresponding phosphonium salt. Treatment of the salt with sodium acetate yielded the novel PCO phosphine **1**, which was purified by chromatography on a silica column.

Scheme 1

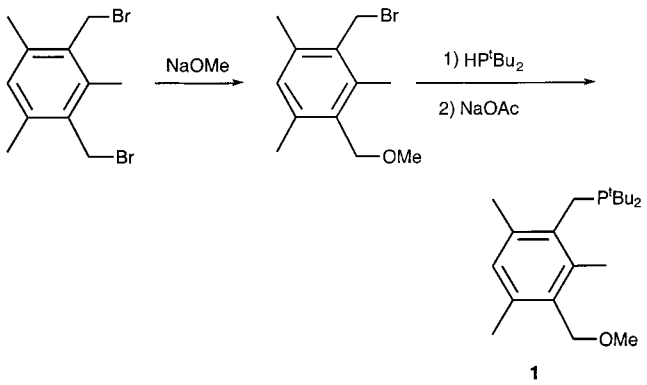

1

Carbon−Hydrogen Bond Activation. Cationic rhodium(I) precursors, $[Rh(coe)_2(solv)_n]BF_4$ (solv = solvent; coe = cyclooctene), were obtained by chloride abstraction from $[Rh(coe)_2Cl]_2$ according to a known procedure.[12] When $[Rh(coe)_2(solv)_n]BF_4$ was reacted at room temperature with the ligand **1** in THF, acetone, or methanol, quantitative formation of the C−H activation products **2**, **3**, and **4**, respectively, was observed within 1 h (Scheme 2).

Complexes **3** and **4** are stable, while **2** gradually decomposes in THF. **2**, **3**, and **4** immediately decompose when dissolved in noncoordinating solvents, such as benzene. NMR spectra of a THF solution of **2** indicate the formation of a C−H activation product, which gives rise to a broad doublet at 125.5 ppm ($^1J_{RhP}$ = 193.9 Hz) in $^{31}P\{^1H\}$ NMR; the hydride signal appears as a broad signal at −27.0 ppm in ^1H NMR, more detailed characterization being impeded by decomposition. In acetone or methanol, two different C−H activation products are formed, namely an "open-arm" (noncoordinated methoxy) and a "closed-arm" (coordinated methoxy) species. In acetone-d_6, the $^{31}P\{^1H\}$ NMR spectrum exhibits two signals: a doublet at 130.4 ppm ($^1J_{RhP}$ = 192.2 Hz) and a doublet at 126.5 ppm ($^1J_{RhP}$ = 191.5 Hz), with an integrated peak area ratio of 4.4. In the ^1H NMR spectrum, two signals due to the hydride ligand bonded to rhodium appear: a broad signal at −24.70 ppm and a doublet of doublets at −24.89 ppm ($^1J_{RhH}$ = 27.2 Hz, $^2J_{PH}$ = 18.1 Hz). The methylene hydrogens of the methoxy arm, which is coordinated to the metal, are diastereotopic and appear as an AB quartet, the splitting pattern being typical of a sidearm methylene involved in chelation in a bis-chelating pincer system, such as PCP and PCN.[7] Thus, the ratio between the "open-arm" and "closed-arm" structures (complexes **3a** and **3b**, respectively) is most clearly evaluated from the ^1H NMR spectrum by observing the ratio between the AB quartet—comprising two doublets at 5.0 and 4.6 ppm ($^2J_{HH}$ = 12.5 Hz), and representing the "closed-arm" form, complex **3b**—and the singlet at 4.4 ppm, which represents the "open-arm" form, complex **3a**. The observed ratio of **3b**:**3a** = 4.4 indicates that the "closed-arm" form **3b** prevails in acetone. The main spectral features of complex **4** (in methanol) are similar to those of **3** (in acetone). In methanol, the "open-arm" complex prevails, resulting in a ratio of **4a**:**4b** = 1.5, in agreement with theoretical calculations (vide infra).

Two "open-arm" C−H activation products are in principle possible, resulting from the activation of the two different methyl

(6) (a) Gozin, M.; Weisman, A.; Ben-David, Y.; Milstein, D. *Nature* **1993**, *364*, 699. (b) Gozin, M.; Aizenberg, M.; Liou, Sh.-Y.; Weisman, A.; Ben-David, Y.; Milstein, D. *Nature* **1994**, *370*, 42. (c) Liou, Sh.-Y.; Gozin, M.; Milstein, D. *J. Am. Chem. Soc.* **1995**, *117*, 9774. (d) Liou, Sh.-Y.; Gozin, M.; Milstein, D. *J. Chem. Soc., Chem. Commun.* **1995**, 1965. (e) van der Boom, M. E.; Kraatz, H.-B.; Ben-David, Y.; Milstein, D. *J. Chem. Soc., Chem. Commun.* **1996**, 2167. (f) van der Boom, M. E.; Liou, Sh.-Y.; Ben-David, Y.; Milstein, D. *J. Am. Chem. Soc.* **1998**, *120*, 13415. (g) Liou, Sh.-Y.; van der Boom, M. E.; Milstein, D. *Chem. Commun*. **1998**, 687. (h) van der Boom, M. E.; Ben-David, Y.; Milstein, D. *Chem. Commun.* **1998**, 917. (i) van der Boom, M. E.; Kraatz, H.-B.; Hassner, L.; Ben-David, Y.; Milstein, D. *Organometallics* **1999**, *18*, 3873. (j) Cohen, R.; van der Boom, M. E.; Shimon, L. J. W.; Rozenberg, H.; Milstein, D. *J. Am. Chem. Soc.* **2000**, *122*, 7723. (k) Rybtchinski, B.; Milstein, D. *J. Am. Chem. Soc.* **1999**, *121*, 4528. (l) Gauvin, R. M.; Rozenberg, H.; Shimon, L. J. W.; Milstein, D. *Organometallics* **2001**, *20*, 1719.

(7) (a) Rybtchinski, B.; Vigalok, A.; Ben-David, Y.; Milstein, D. *J. Am. Chem. Soc.* **1996**, *118*, 12406. (b) Gandelman, M.; Vigalok, A.; Shimon, L. J. W.; Milstein, D. *Organometallics* **1997**, *16*, 3981.

(8) Sundermann, A.; Uzan, O.; Milstein, D.; Martin, J. M. L. *J. Am. Chem. Soc.* **2000**, *122*, 7095.

(9) Gandelman, M.; Vigalok, A.; Milstein, D. *J. Am. Chem. Soc.* **2000**, *117*, 9774.

(10) Rybtchinski, B.; Konstantinovsky, L.; Shimon, L. J. W.; Vigalok, A.; Milstein D. *Chem. Eur. J.* **2000**, *17*, 3287.

(11) van der Made, A. W.; van der Made, R. H. *J. Org. Chem.* **1993**, *58*, 1262.

Scheme 2

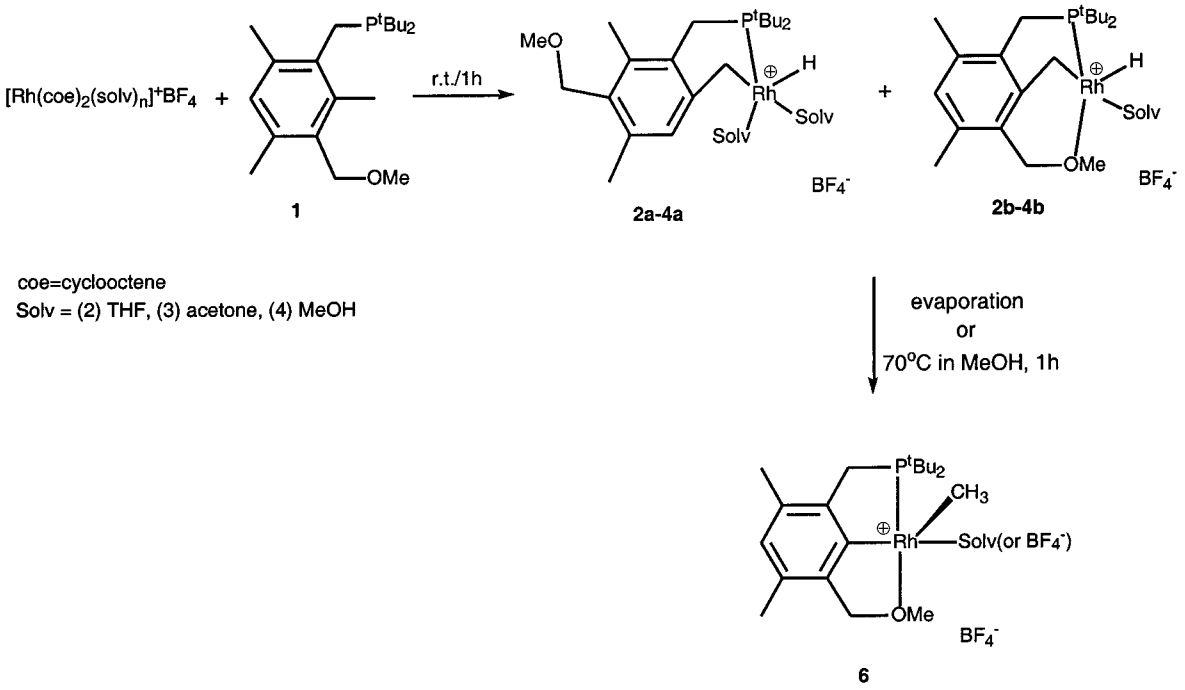

groups: one structure in which the methoxy arm is located at the ortho position to the methylene bridge, and the other in which it is located at the para position to the bridge. In the former case the "open-arm" form is expected to be in equilibrium with the "closed-arm" one, because the methoxy arm is in close proximity to the rhodium center. On the other hand, the latter structure has the methoxy arm on the opposite side of the aromatic ring. Hence, for this "open-arm" form to be in equilibrium with the other "open-arm" species—let alone the "closed-arm" form—it is necessary for the methylene bridge to be completely detached from the metal center (via reductive elimination). Only then can the aromatic ring rotate about the $Ar-CH_2P$ bond, permitting the methoxy moiety to come within coordination distance.

The identity of **4a** in methanol was determined by spin saturation transfer (SST) experiments, performed at room temperature. When the hydride ligand of **4a** was irradiated, no spin saturation transfer was detected. On the other hand, it was found by SST that the hydride ligand of the "open-arm" form exchanges with one of the methylene bridge hydrogens,[10] while no exchange takes place with the other methyl groups of the PCO ligand. This means that no full detachment of the C−H activated methyls occurs in both systems. Furthermore, as shown by irradiating the methylene hydrogens of the methoxy arm, no hydrogen exchange appears to take place between the methoxy arms of the "open-arm" and "closed-arm" forms. This indicates that there is no equilibrium between the two species on the time scale of the experiment. Thus, once C−H activation takes place, the products **4a** and **4b** do not interconvert. It is therefore concluded that the "open-arm" structure consistent with the above observations is **4a**, in which the methoxy arm is located para to the methylene bridge. The ratio between the "open-arm" and "closed-arm" forms is likely to be determined by the competition between the methoxy arm and the solvent with respect to coordination to the metal center and by the barrier for C−H activation with these species. Complex **4a**, with its methoxy arm in the para position, very closely resembles—both in structure and in behavior—complex **5** which was recently reported by us.[10]

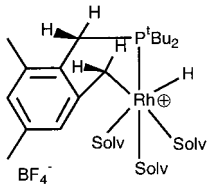

5

SST experiments performed on a methanol solution of complex **5** showed results very similar to those obtained for complex **4a**. Exchange between the hydride ligand and the methylene bridge hydrogens of complex **5** was found to occur at room temperature, whereas exchange with the other methyl group occurred only at higher temperatures (above 35 °C in methanol). This was attributed to agostic bonding between the metal and C−H bonds of the methyl group formed upon reductive elimination, preventing complete detachment of this group at room temperature. Thus, C−H activation of the two methyl groups ortho to the phosphine arm in complex **4** to produce compounds **4a**,**b**, which are stable at room temperature and do not interconvert, is expected, on the grounds of the similarity of complex **4** to complex **5**.

Carbon−Carbon Bond Activation. When a solution of the C−H activation products **4** in methanol is heated to about 70 °C, the complexes are transformed into the C−C activation product **6**. The process is rather rapid, with 50% conversion taking place within 15 min (determined by $^{31}P\{^1H\}$ NMR). However, prolonged heating results in considerable decomposition, such that the reaction is not quantitative (85% yield by $^{31}P\{^1H\}$ NMR). Formation of the C−C activation products very likely takes place also in acetone and THF after heating, but the reaction gives rise to many decomposition products, and appropriate characterization could not be accomplished. The $^{31}P\{^1H\}$ NMR spectrum of **6** in methanol exhibits only one signal, a doublet at 90.2 ppm ($^1J_{RhP}$ = 190.8 Hz), in contrast to the

(12) Schrock, R. R.; Osborn, J. A. *J. Am. Chem. Soc.* **1971**, *93*, 3089.

two low-field signals of the C−H activation product mixture. The ^{1}H NMR spectrum shows a doublet at 1.02 ppm ($^2J_{RhH}$ = 2.3 Hz), which corresponds to the hydrogen atoms of the methyl bound to rhodium. This moiety also gives rise to a doublet of doublets in the ^{13}C{^{1}H} NMR spectrum, located at −4.55 ppm ($^1J_{RhC}$ = 32.0 Hz, $^2J_{PC}$ = 8.3 Hz). The same spectrum also shows a doublet of doublets at 157.02 ppm ($^1J_{RhC}$ = 35.7 Hz, $^2J_{PC}$ = 4.7 Hz), which corresponds to the aromatic carbon atom to which the metal is bound (the ipso carbon atom). The difference between complexes **4** and **6** is also highlighted by electrospray mass spectrometry. Although **4** and **6** exhibit a molecular cation peak at practically the same location, with *m*/*e* 425.37 (no solvent or BF_4 is present), their fragmentation pattern is markedly different. The spectrum of **6** shows several significant peaks, the most notable of which is at *m*/*e* 411.35, with over 50% intensity, indicating loss of a methyl group. In the mass spectrum of **4**, on the other hand, the molecular peak is the only significant one. The structure of complex **6** was confirmed by an X-ray structural study (vide infra). The fact that heating converts the C−H activation complex **4** into the C−C cleavage product **6**, and that continued heating increases the ratio of C−C to C−H activation products, clearly indicates that the C−C activation product is the thermodynamically more stable of the two complexes. On the other hand, the fact that reaction between [Rh(coe)$_2$(solv)$_n$]BF_4 and ligand **1** yields only C−H activation products at room temperature—in all solvents used—implies that C−H activation is kinetically favored over C−C activation. Thus, in the Rh−PCO system selective formation of kinetic C−H activation products takes place at room temperature, while selective rhodium insertion into a C−C bond can be achieved under mild heating. Significantly, whereas C−H activation of the two methyl groups is observed, only the C−C bond between the chelating arms is activated, demonstrating that the chelating methoxy ligand is both essential and sufficient for C−C activation in this system.

An attempt to isolate the C−H activation products led to a very intriguing observation: removal of the solvent from a solution of the C−H activation complexes **2**−**4** under vacuum for several days resulted in conversion of the C−H to the C−C activation product. This result, which has not been observed elsewhere so far, suggests that the system is very sensitive to the presence of a solvent. Our X-ray structural studies and computational results suggest that this is due to a special effect of BF_4^- anion coordination, which takes place upon solvent evaporation (vide infra). An interesting result supporting the effect of solvent removal was obtained in the presence of ethylene glycol. As in the case of methanol, heating an acetone solution of the C−H activation products at 70−80 °C in the presence of ethylene glycol is required in order to achieve C−C activation. However, upon evaporation, C−C bond activation does not take place. Ethylene glycol was observed to remain coordinated to the metal center after the evaporation under high vacuum, most probably due to its chelation to the metal. It is known that ethylene glycol can be a chelating ligand for cationic rhodium centers.[10]

X-ray Crystallographic Study of Complex 6. Crystals of complex **6** suitable for X-ray analysis were grown from an ether extract of the dry complex **6** at room temperature. The rhodium atom is centered at the base of a slightly distorted square pyramid, with the methyl group at the apex (Figure 1). The C(1)−Rh−X bond angles are close to 90° (X = C(3), O(4), F(3) or P(2)): C(1)−Rh−C(3) = 88.71°, C(1)−Rh−O(4) = 92.93°, C(1)−Rh−F(3) = 89.92°, C(1)−Rh−P(2) = 97.29°). The methyl group is situated trans to the empty coordination site, with a Rh−CH_3 bond length of 2.02 Å. The aromatic ring is linked to the rhodium center via the ipso carbon atom, with a Rh−C_{Ar} bond length of 1.95 Å. The chelating sidearms of the PCO ligand are coordinated to the metal atom through oxygen and phosphorus, with bond lengths of 2.15 Å for Rh−O and 2.22 Å for Rh−P. Finally, the position trans to the ipso carbon is occupied by BF_4^-, which is coordinated to the rhodium atom via one of the fluorine atoms, F(3). The length of the Rh−F(3) bond is 2.27 Å. Furthermore, the existence of this bond is supported by the fact that the B−F(3) bond is longer than the other B−F bonds: 1.44 vs 1.36−1.38 Å, respectively. To the best of our knowledge, no crystal structures containing Rh−FBF3 bonds have been reported.[13] Such a bond between the rhodium atom and the weakly coordinating anionic ligand BF_4^- is not common.[13,14]

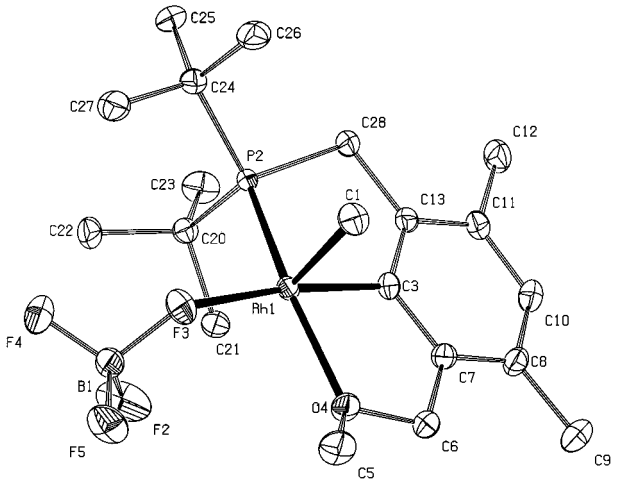

Figure 1. ORTEP plot of the X-ray structure of the closed-arm CC activation product with BF_4^- counterion, **6**.

Comparison of the PCO and PC Ligand Systems. Important insight into the mode of reactivity of the PCO−Rh system is obtained by a comparison to the PC complex **5** (vide supra). As mentioned above, the latter complex is very similar sterically and electronically to the "open-arm" form of the PCO complex. However, the PC system differs markedly from the PCO regarding bond activation. In the PC system, only C−H bond activation takes place, resulting in complex **5**; this process is reversible. In striking contrast with the PCO system, the C−H activation product **5** is stable toward evaporation of the solvent and is not transformed into a C−C activation product. Furthermore, no C−C bond activation was observed upon heating of a solution of **5** in THF, acetone, or methanol. The exclusive activation of the C−C bond situated between the phosphine and methoxy arm and the absence of C−C activation in the PC system suggest *that chelation is crucial for C−C bond activation*. Significantly, the methoxy group, although weakly coordinating in comparison to phosphines and amines, promotes C−C bond activation when it is involved in chelation. Apparently, the chelate effect influences both the kinetics and thermodynamics of the process. An important kinetic factor is the bonding of the metal center by the two ligand arms, which brings the metal into close proximity to the C−C bond to be cleaved. The resulting C−C activation product is then significantly stabilized by the presence of two five-membered chelate rings, creating a thermodynamic driving force for the reaction.

(13) For an example of a Rh−FBF3 bond characterized in solution, see: Sutherland, B. R.; Cowie, M. *Inorg. Chem.* **1984**, *23*, 1290.

(14) Beck, W.; Sünkel, K. *Chem. Rev.* **1988**, *88*, 1405−1421.

Scheme 3

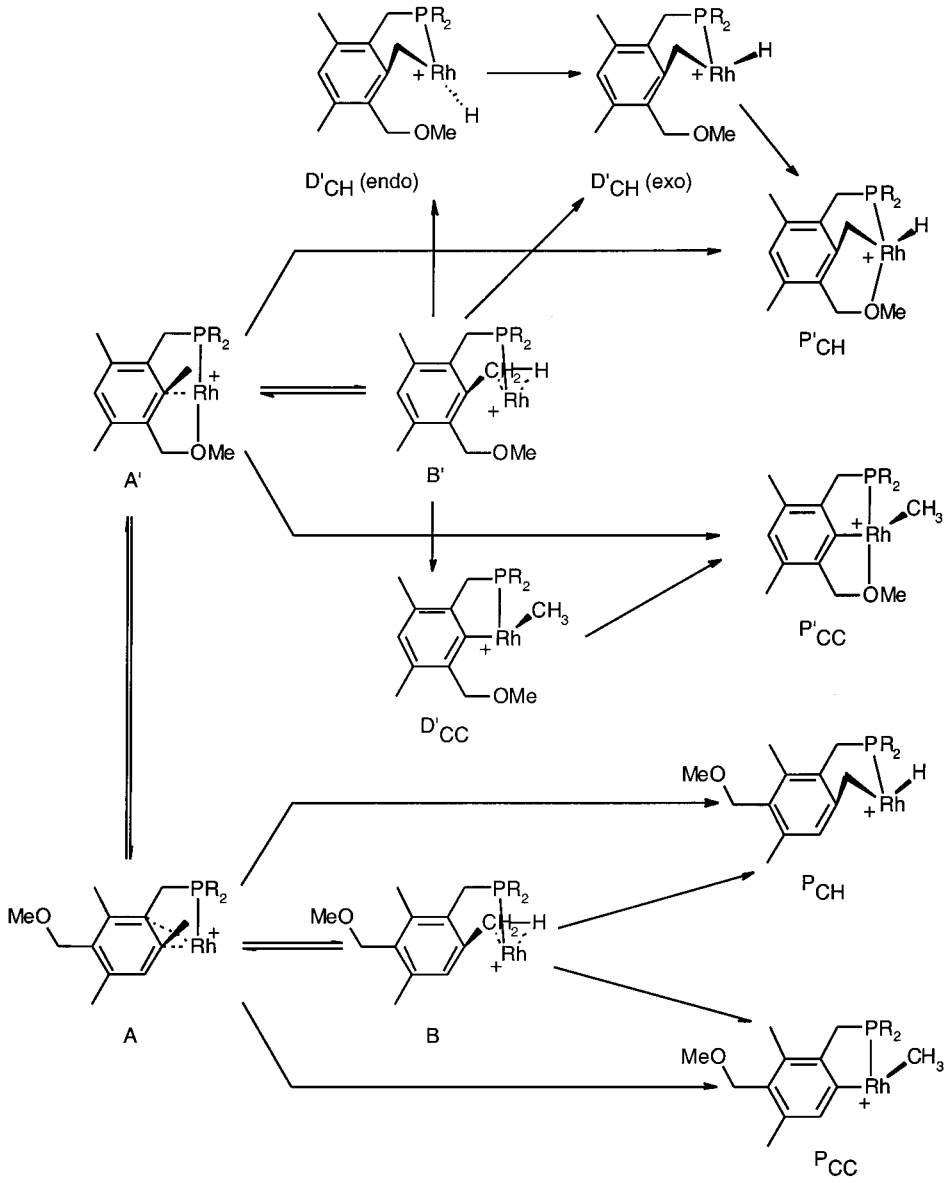

Further insight regarding these factors was obtained from the computational study of the Rh−PCO system.

Computational Results

To understand the reactivity of the PCO system with the cationic rhodium(I) precursor, which at room temperature selectively cleaves the C−H bond in the "open-arm" and "closed-arm" systems and leads exclusively to C−C cleavage in the "closed-arm" system in the absence of solvent or upon heating, we explored a variety of reaction pathways.

Possible Reaction Pathways without Solvent Ligands. For a reaction pathway involving the C−H and C−C products, we found 26 stationary points on the energy hypersurface (Scheme 3). Computed barrier heights, reaction energies, and ligand stabilization energies at all levels of theory considered by us are given in Tables 1, 2, and 3, respectively. Our discussion here will be in terms of the ONIOM(mPW1K/lanl2dz+p: mPW1K/lanl2dz) values, which we deem to be the most reliable. (See below for a comparison of the different levels of theory.) Unless stated otherwise, we will be referring to free energies at room temperature (ΔG_{298}). For easy reference, reaction profiles at the "bottom of the well" (ΔE_e) at all three levels of theory haven been given in Figures 2, 3, and 4, while ΔH_{298} and ΔG_{298} profiles at our best level of theory (mPW1K/lanl2dz+p) have been given in Figures 5, 6, and 7, respectively.

The Intermediate Structures. The reaction of the PCO ligand with the mononuclear cationic Rh(I) olefin complex results in ligand substitution which takes place prior to the bond activation. Of the four possible entry channels **A**, **A′**, **B**, and **B′** which could act as common intermediates, we found the Rh(I) complexes **A** and **A′** to be more stable than their agostic counterparts **B** and **B′**. The local minima **A** and **A′** are common intermediates, from which both C−H and C−C activation are possible. In the "closed-arm" intermediate **A′**, a tricoordinate (T-shaped) rhodium is found, with the phosphine and methoxy ligands acting as the two "arms" of the T. The complex is slightly stabilized by a weak η^1 interaction with the ipso carbon of the phenyl ring. In the "open-arm" intermediate **A**, only the phosphine "arm" is present, but the rhodium is η^2 bound to the ring, specifically to the ipso carbon and the ortho carbon on the phosphorus side. Some weak interaction, in addition, exists with the facing ortho and meta carbons, but both the Wiberg bond orders and an electron density plot (see Supporting

Table 1. Computed Reaction Barrier Heights (kcal·mol^{-1})

	B3LYP/lan2dz				B3LYP/lanl2dz+p	mPW1K/lanl2dz+p	
	$\Delta E^{\#}_e$	$\Delta E^{\#}_0$	$\Delta H^{\#}_{298}$	$\Delta G^{\#}_{298}$	$\Delta E^{\#}_e$	$\Delta E^{\#}_e$	$\Delta G^{\#}_{298}$[a]
Pathways without MeOH Spectator Ligands							
$\mathbf{P}_{CC}\rightarrow\mathbf{A}$	35.5	35.6	35.2	36.5	31.0	26.5	27.5
$\mathbf{A}\rightarrow\mathbf{P}_{CC}$	26.9	25.2	25.1	25.3	25.6	30.9	29.3
$\mathbf{A}\rightarrow\mathbf{A'}$	1.7	1.6	1.1	2.7	1.9	0.6	1.6
$\mathbf{A'}\rightarrow\mathbf{A}$	13.9	13.5	13.0	14.1	8.0	5.3	5.5
$\mathbf{A'}\rightarrow\mathbf{P'}_{CC}$	10.9	9.7	9.2	11.0	11.3	12.3	12.4
$\mathbf{P'}_{CC}\rightarrow\mathbf{A'}$	35.1	35.0	34.5	36.1	32.3	28.1	29.1
$\mathbf{P}_{CH}\rightarrow\mathbf{A}$	28.6	27.7	27.7	27.3	24.0	19.4	18.1
$\mathbf{A}\rightarrow\mathbf{P}_{CH}$	16.9	14.4	14.0	14.4	16.0	18.5	16.1
$\mathbf{A'}\rightarrow\mathbf{P'}_{CH}$	10.5	8.3	7.5	9.8	11.2	9.8	9.1
$\mathbf{P'}_{CH}\rightarrow\mathbf{A'}$	26.5	25.7	25.5	25.8	24.4	19.8	19.0
$\mathbf{A}\rightarrow\mathbf{B}$	16.1	15.4	15.1	15.6	15.6	16.5	16.1
$\mathbf{B}\rightarrow\mathbf{A}$	4.2	4.3	4.0	5.1	3.5	4.7	5.7
$\mathbf{B'}\rightarrow\mathbf{A'}$	24.0	22.9	22.4	23.2	18.8	18.9	18.1
$\mathbf{A'}\rightarrow\mathbf{B'}$	2.3	2.1	1.7	2.8	2.4	2.5	3.0
Pathways with One MeOH Spectator Ligand							
$\mathbf{P}_{CC}\rightarrow\mathbf{A}$	32.6	32.4	32.0	33.2	29.7	25.4	26.1
$\mathbf{A}\rightarrow\mathbf{P}_{CC}$	24.5	23.1	22.9	23.5	26.2	30.4	29.4
$\mathbf{A}\rightarrow\mathbf{AA'}$	3.4	3.7	3.0	5.7	3.1	2.7	5.0
$\mathbf{AA'}\rightarrow\mathbf{A}$	12.6	12.2	11.7	12.7	6.8	5.5	5.6
$\mathbf{A'}\rightarrow\mathbf{P'}_{CC}$	10.5	9.3	8.8	10.4	11.0	12.5	12.4
$\mathbf{C'}_{CC}\rightarrow\mathbf{A'}$	30.7	31.1	30.4	32.6	28.5	25.1	27.0
$\mathbf{P}_{CH}\rightarrow\mathbf{A}$	26.3	25.6	26.1	24.6	23.9	19.4	17.7
$\mathbf{A}\rightarrow\mathbf{P}_{CH}$	12.0	9.8	9.3	10.2	15.0	16.9	15.1
$\mathbf{A'}\rightarrow\mathbf{P'}_{CH}$	8.1	6.0	5.3	6.7	10.2	10.8	9.3
$\mathbf{P'}_{CH}\rightarrow\mathbf{A'}$	18.7	18.3	18.0	18.9	17.8	14.7	14.9
Pathways with Two MeOH Spectator Ligands							
$\mathbf{P}_{CC}\rightarrow\mathbf{A}$	27.2	27.2	26.7	28.4	24.5	21.3	22.5
$\mathbf{A}\rightarrow\mathbf{P}_{CC}$	18.2	16.8	16.8	17.4	17.3	20.2	19.4
$\mathbf{P}_{CH}\rightarrow\mathbf{A}$	18.4	17.9	17.8	18.0	16.1	13.5	13.1
$\mathbf{A}\rightarrow\mathbf{P}_{CH}$	4.1	2.0	1.7	2.3	3.9	5.5	3.7

[a] Using the additivity approximation $\Delta G^{\#}_{298}$[mPW1K] $\approx \Delta E^{\#}_e$ [mPW1K/lanl2dz+p] + $\Delta G^{\#}_{298}$[B3LYP/lanl2dz] − $\Delta E^{\#}_e$ [B3LYP/lanl2dz].

Table 2. Computed Reaction Energies with Respect to the Relevant Intermediates (kcal·mol^{-1})

	B3LYP/lan2dz				B3LYP/ lanl2dz+p	mPW1K/lanl2dz+p	
	ΔE_e	ΔE_0	ΔH_{298}	ΔG_{298}	ΔE_e	ΔE_e	ΔG_{298}
Without MeOH Spectator Ligands							
$\mathbf{P}_{CC}-\mathbf{A}$	−8.6	−10.4	−10.1	−11.2	−5.4	4.3	1.8
$\mathbf{P}_{CH}-\mathbf{A}$	−11.7	−13.3	−13.6	−12.8	−8.0	−0.9	−2.0
$\mathbf{B}-\mathbf{A}$	11.8	11.1	11.1	10.5	12.0	11.8	10.4
$\mathbf{A}-\mathbf{A'}$	−12.2	−11.9	−11.9	−11.5	−6.2	−4.6	−4.0
$\mathbf{P'}_{CC}-\mathbf{A'}$	−24.2	−25.3	−25.3	−25.1	−21.0	−15.8	−16.7
$\mathbf{P'}_{CH}-\mathbf{A'}$	−16.1	−17.4	−18.0	−16.0	−13.2	−9.9	−9.9
$\mathbf{B'}-\mathbf{A'}$	21.7	20.9	20.7	20.4	16.5	16.4	15.1
With One MeOH Spectator Ligand							
$\mathbf{P}_{CC}-\mathbf{A}$ + 1MeOH	−8.1	−9.3	−9.1	−9.7	−3.4	5.0	3.3
$\mathbf{P}_{CH}-\mathbf{A}$ + 1MeOH	−14.4	−15.8	−16.7	−14.5	−8.9	−2.5	−2.6
$\mathbf{B}-\mathbf{A}$ + 1MeOH	6.1	6.5	6.2	6.9	7.9	10.3	11.0
$\mathbf{A}-\mathbf{A'}$ + 1MeOH	−9.2	−8.5	−8.7	−7.1	−3.7	−2.8	−0.6
$\mathbf{P'}_{CH}-\mathbf{A'}$ + 1MeOH	−10.5	−12.3	−12.6	−12.2	−7.6	−4.0	−5.6
$\mathbf{P'}_{CC}-\mathbf{A'}$ +1MeOH	−20.2	−21.8	−21.7	−22.3	−17.4	−12.5	−14.6
$\mathbf{B'}-\mathbf{A'}$ + 1MeOH	13.3	13.0	12.8	12.5	9.9	11.2	10.3
With Two MeOH Spectator Ligands							
$\mathbf{P}_{CC}-\mathbf{A}$ + 2MeOH	−8.9	−10.4	−9.9	−11.0	−7.2	−1.0	−3.1
$\mathbf{P}_{CH}-\mathbf{A}$ + 2MeOH	−14.2	−16.0	−16.1	−15.7	−12.2	−8.0	−9.4
$\mathbf{A}(MeOH)_2 \rightarrow \mathbf{A'}(MeOH)$ + MeOH	−15.4	−12.9	−13.4	−1.2	−8.8	−8.8	5.4

[a] Using the additivity approximation: $\Delta G^{\#}_{298}$[mPW1K] $\approx \Delta E^{\#}_e$[mPW1K/lanl2dz+p] + $\Delta G^{\#}_{298}$[B3LYP/lanl2dz] − $\Delta E^{\#}_e$[B3LYP/lanl2dz].

Information) reveal that the interaction with the phenyl ring predominantly has η^2 rather than η^4 character. **A** is found to be 4.0 kcal·mol^{-1} less stable than **A′** because of missing stabilization by the methoxy coordination. Perspective views of structures **A** and **A′**, with and without added MeOH ligands (vide infra), can be found in Figure 8.

η^1 and η^2 coordination in the PCO system are greatly favored over the formation of an agostic bond. The C−H agostic intermediates **B** and **B′** are destabilized by 10.4 kcal·mol^{-1} for the open-arm system and 15.1 kcal·mol^{-1} for the closed-arm system. In both cases, aside from the C−H agostic interaction, only the phosphine "arm" is attached to the rhodium. Since no interaction between the methoxy group and the rhodium could be found in either case**,** both C−H agostic intermediates are almost isoergonic ($\Delta\Delta G$ = 0.6 kcal·mol^{-1}). Apparently, the methoxy "arm" in **B′** is too short to permit an optimal interaction of the chelated rhodium atom with the C−H bonds of the methyl group. Because the C−OMe as well as the Rh−O bonds are shorter than the corresponding bonds in the phosphine "arm", the rhodium is forced to be close to the phenyl ring, and therefore the tricoordinate (T-shape) η^1 complex is favored in intermediate **B′**. Intermediate **B** favors the η^2 coordination for

Table 3. Computed Association Energies (kcal·mol^{-1}) for One and Two MeOH Spectator Ligands

	B3LYP/lanl2dz				B3LYP/lan2dz+p	mPW1K/lanl2dz+p	
	ΔE_e	ΔE_0	ΔH_{298}	ΔG_{298}	ΔE_e	ΔE_e	ΔG_{298}
			First Association Energies				
TS-AP$_{CC}$ + 1MeOH	−25.1	−22.7	−22.8	−11.8	−19.5	−22.4	−9.1
TS-AP$_{CC}$ + 1MeOH	−28.1	−26.0	−26.0	−15.1	−20.8	−23.5	−10.5
A + 1MeOH	−25.7	−23.9	−23.7	−13.3	−21.5	−23.1	−10.7
TS-AP$_{CH}$ + 1MeOH	−30.6	−28.5	−28.5	−17.6	−22.5	−24.7	−11.7
P$_{CH}$ + 1MeOH	−28.4	−26.4	−26.9	−14.9	−22.4	−24.7	−11.2
B + 1MeOH	−31.4	−28.5	−28.7	−16.9	−25.7	−24.6	−10.1
P′$_{CC}$ + 1MeOH	−18.7	−17.0	−16.9	−6.1	−15.5	−17.9	−5.2
TS-P′P′$_{CC}$ + 1MeOH	−23.1	−20.9	−21.0	−9.5	−19.3	−21.0	−7.4
A′ + 1MeOH	−22.7	−20.5	−20.6	−8.9	−19.0	−21.2	−7.3
TS-A′P′$_{CH}$ + 1MeOH	−25.1	−22.8	−22.7	−12.0	−20.0	−20.3	−7.2
P′$_{CH}$ + 1MeOH	−17.2	−15.4	−15.2	−5.1	−13.3	−15.2	−3.1
TS-AA′ + 1MeOH	−24.0	−21.8	−21.8	−10.2	−20.2	−21.0	−7.3
B′ + 1MeOH	−33.4	−30.4	−30.1	−19.6	−27.9	−29.0	−15.1
			Second Association Energies				
P$_{CC}$ + 2MeOH	−16.3	−14.0	−14.2	−2.4	−12.5	−14.9	−1.0
TS-AP$_{CC}$ + 2MeOH	−21.7	−19.2	−19.5	−7.2	−17.7	−19.0	−4.6
A + 2MeOH	−15.4	−12.9	−13.4	−1.2	−8.8	−8.8	5.4
TS-AP$_{CH}$ + 2MeOH	−23.3	−20.8	−21.0	−9.0	−19.9	−20.3	−6.0
P$_{CH}$ + 2MeOH	−15.3	−13.1	−12.7	−2.4	−12.1	−14.3	−1.4

[a] Using the additivity approximation $\Delta G^{\#}_{298}$[mPW1K] ≈ $\Delta E^{\#}_{e}$[mPW1K/lanl2dz+p] + $\Delta G^{\#}_{298}$[B3LYP/lanl2dz] − $\Delta E^{\#}_{e}$[B3LYP/lanl2dz].

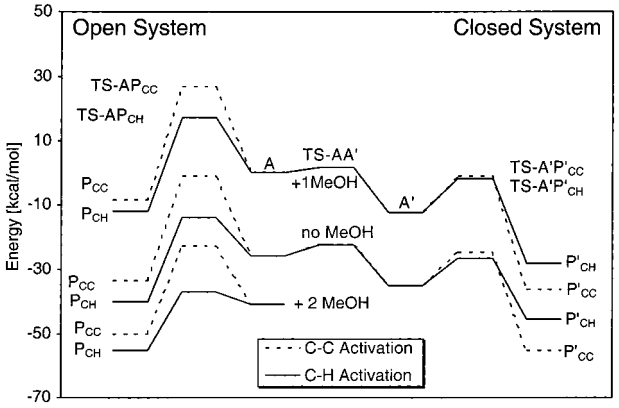

Figure 2. B3LYP/lanl2dz computed ΔE_e reaction profiles for competing closed-arm and open-arm C−C and C−H activation routes with and without MeOH spectator ligands.

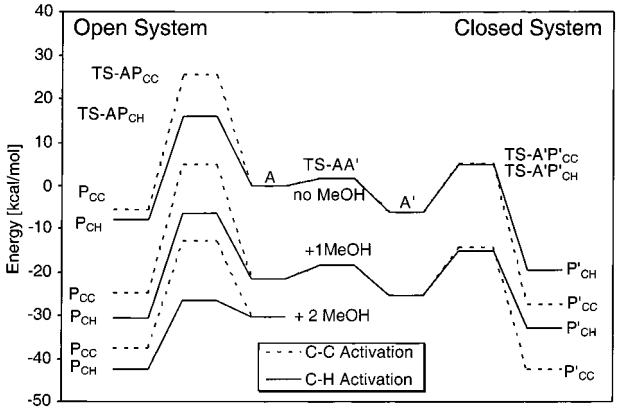

Figure 3. B3LYP/lanl2dz+p computed ΔE_e reaction profiles for competing closed-arm and open-arm C−C and C−H activation routes with and without MeOH spectator ligands.

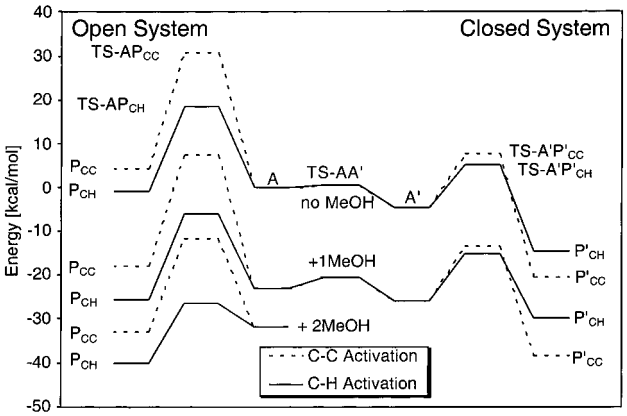

Figure 4. mPW1K/lanl2dz+p computed ΔE_e reaction profiles for competing closed-arm and open-arm C−C and C−H activation routes with and without MeOH spectator ligands.

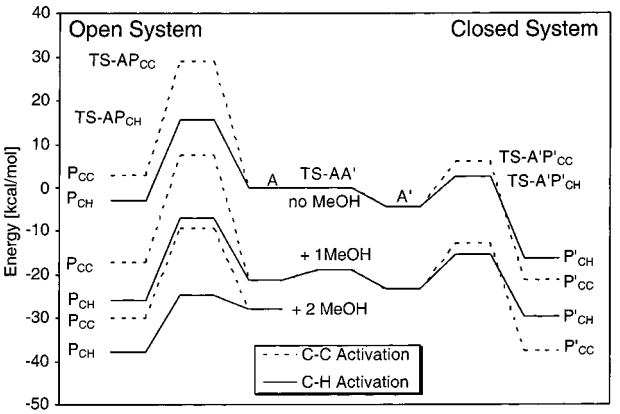

Figure 5. mPW1K/lanl2dz+p computed ΔH_{298} reaction profiles for competing closed-arm and open-arm C−C and C−H activation routes with and without MeOH spectator ligands.

electronic reasons. More electron density can thus be donated to the rhodium than by a C−H agostic bond.

There are now two potential pathways from here to the C−C and C−H activated products. One could go directly from the η^2 and (T-shape) η^1 complexes **A** and **A′** to their respective activated product pairs {**P**$_{CC}$, **P**$_{CH}$} and {**P′**$_{CC}$, **P′**$_{CH}$}; this route shall be termed the "direct pathway". The other alternative proceeds via the above-mentioned C−H agostic intermediates **B** and **B′**; we shall call this the "agostic pathway". The first barriers on the agostic pathways are the ones for the formation of **B** and **B′**, and they are found to be 16.1 kcal·mol^{-1} for **B** and 18.2 kcal·mol^{-1} for **B′**. As the barriers for the back-reactions

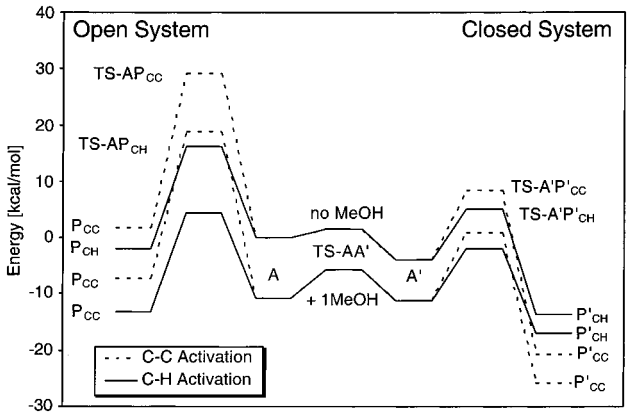

Figure 6. mPW1K/lanl2dz+p computed ΔG_{298} reaction profiles for competing closed-arm and open-arm C−C and C−H activation routes with and without MeOH spectator ligands.

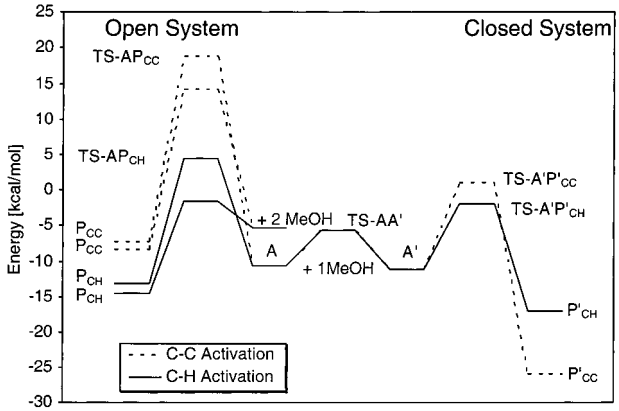

Figure 7. mPW1K/lanl2dz+p computed ΔG_{298} reaction profiles for competing closed-arm and open-arm C−C and C−H activation routes with one and two MeOH spectator ligands.

are by far smaller (5.7 and 3.1 kcal·mol^{-1} for the open-arm and closed-arm systems, respectively), the direct pathways are naturally favored.

The η^2 complexes are connected on the energy hypersurface via the transition states for C−C activation (**TS-AP**$_{CH}$, **TS-A′P′**$_{CC}$), their counterparts for C−H activation (**TS-AP**$_{CH}$, **TS-A′P′**$_{CH}$), and the transition state (**TS-AA′**) for interconversion between **A** and **A′**. The outcome of our calculations is that, with no solvent molecule coordinated to the rhodium center, C−C activation cannot occur at room temperature with the "open-arm" system due to the large barrier height of 29.3 kcal·mol^{-1}. The barrier of the C−H activation is 16.1 kcal·mol^{-1}; i.e., the activation process is feasible at room temperature. Compared to the C−H activation barrier calculated for the "open-arm" system, the barrier appears to be almost twice as high. This is in disagreement with the observed product ratio in C−H activation. The C−H and C−C products are nearly isoergonic ($\Delta\Delta G = 0.2$ kcal·mol^{-1}).

For the "closed-arm" system, the barrier for C−H activation, 9.1 kcal·mol^{-1}, is 3.3 kcal·mol^{-1} lower than that for C−C activation, 12.4 kcal·mol^{-1}. Both are much lower than the corresponding barriers for the "open-arm" system. Consequently, among the "closed-arm" system products (**P′**$_{CH}$, **P′**$_{CC}$), the C−H product is kinetically favored and the C−C product is thermodynamically favored, being 6.8 kcal·mol^{-1} more stable than the C−H product. Comparison of the barrier heights for the direct and agostic pathways indicates that, considering the above-mentioned rapid back reaction, only the direct pathway will be involved in the reaction. Therefore, the reaction mechanism to be investigated is simplified to the one in Scheme 4.

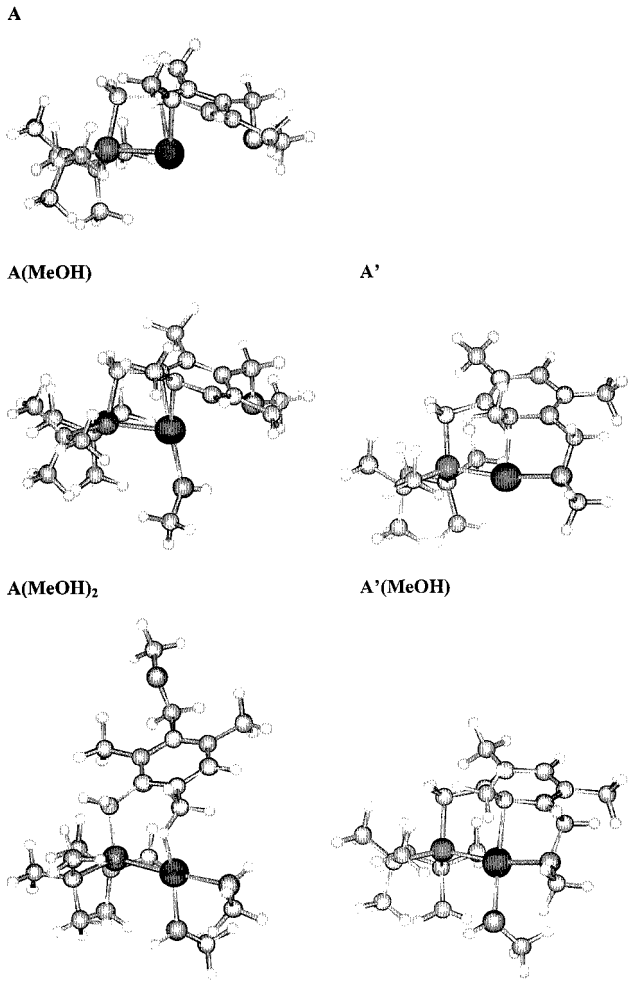

Figure 8. Perspective view of computed structures of the intermediates.

At this point, our calculations explain why no C−C activation is seen for the "open-arm" system; in addition, for the "closed-arm" system, formation of the kinetic C−H product at room temperature and the exclusive formation of the C−C product upon heating can be rationalized. Note that barrier heights for the back-reaction of the C−H products to intermediates **A** and **A′** stand at 18.8 and 19.1 kcal·mol^{-1}, respectively, low enough for C−H formation to be reversible at room temperature. The experimentally observed formation of the "open-arm" system C−H product, however, is in discord with our computational predictions, according to which **P′**$_{CH}$ and **P′**$_{CC}$ are 11.9 and 18.7 kcal·mol^{-1} lower in energy, respectively, than **P**$_{CH}$. We have however, thus far, taken into account neither solvent nor counterion.

Influence of Methanol on the Reaction Profile. The experimental results suggest that the solvent plays a major role in the C−H and C−C bond activation processes. The reactions have been carried out in methanol. Therefore, to a first approximation, we added one methanol "spectator ligand" to each structure and reoptimized all stationary points on the reaction profile (direct pathway) (Scheme 5).

All structures are stabilized by the addition of one methanol molecule. This leads to association energies ranging from 3.1 kcal·mol^{-1} for **P′**$_{CH}$ to 11.7 kcal·mol^{-1} for **TS-AP**$_{CH}$ (see Table 3). As expected, for the closed-arm system the optimized structures for the 14e intermediate **A′** is T-shaped (discounting the fairly weak ring interaction), and for the Rh(III) complexes the C−H as well as the C−C products are square pyramidal (Figure 8). For the closed-arm system, the addition of one methanol molecule does change almost none of both barriers,

Scheme 4

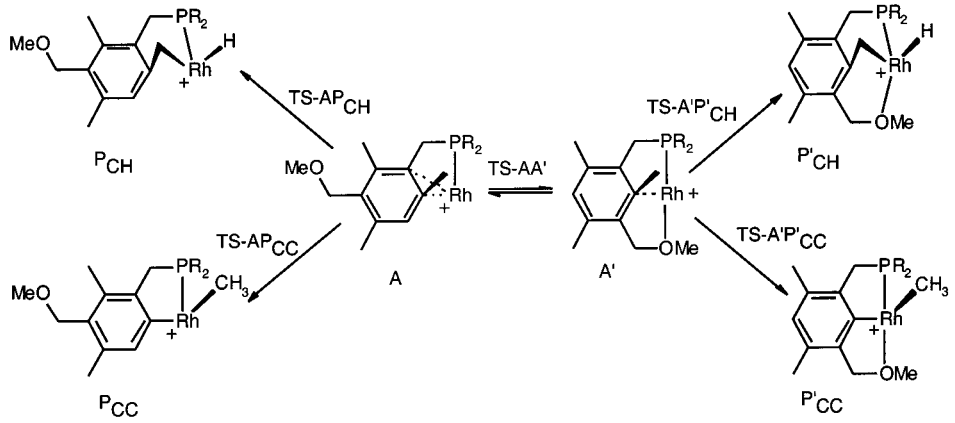

Scheme 5

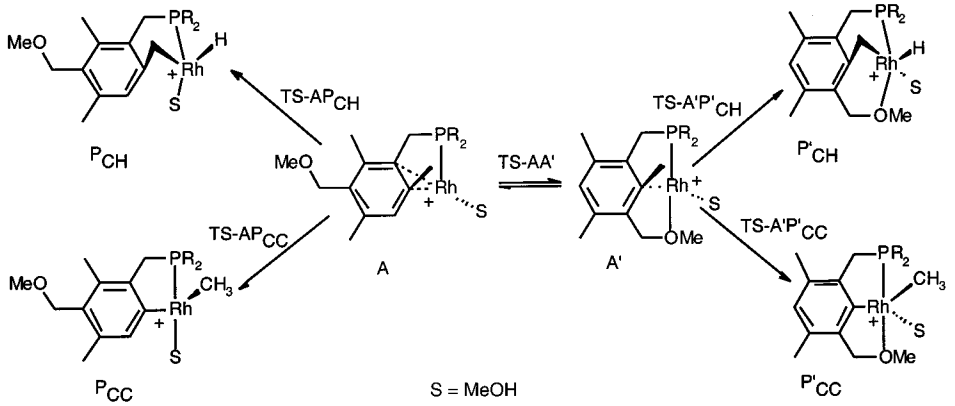

the C−H barrier increases slightly by 0.2 kcal·mol^{-1}, and the C−C barrier remains unchanged. The C−H product is thus kinetically favored by 3.1 kcal·mol^{-1} over the thermodynamic C−C product, which is more stable than the C−H product by 9.0 kcal·mol^{-1}. Therefore, in solution one would expect the kinetic C−H product at room temperature and the thermodynamic C−C product at higher temperature, in agreement with experiment.

In the "open-arm" system, intermediate **A** again shows an η^2 interaction with the phenyl ring. It forms a T-shaped 14-electron complex, with the methanol molecule being trans to the η^2 bond and cis to the phosphine arm. The addition of a solvent molecule stabilizes the complex by 10.7 kcal·mol^{-1}, whereas the association energy for intermediate **A′** is just 7.3 kcal·mol^{-1}. As a result, both intermediates are nearly isoergonic ($\Delta\Delta G$ = 0.8 kcal·mol^{-1}), and the respective interconversion barriers of 5.0 and 5.5 kcal·mol^{-1} are reasonably low. For the "open-arm" system, the addition of one solvent molecule decreases the C−H activation barrier by 1.0 kcal·mol^{-1}, while the C−C activation barrier is basically unchanged. The C−H activation barrier of 15.1 kcal·mol^{-1} appears to be still high compared to the corresponding barrier in the "closed-arm" system. The computational results therefore do not reflect the amount of the C−H product ($\mathbf{P}_{CH}$) formed at room temperature. In contrast, it is easily seen why no open-arm C−C product is formed: it is 5.9 kcal·mol^{-1} less stable than its C−H counterpart, and in fact 3.4 kcal·mol^{-1} less stable than the joint intermediate **A**.

We next explored the effect of addition of second methanol molecule. Attempts to optimize structures for the "closed-arm" systems with a second methanol molecule added invariably led to the latter being evicted or to a structure with the free energy of formation being positive. The "open-arm" system, however, does coordinate a second methanol molecule. Interestingly, this leads to a much greater change of the energy profile than the addition of the first solvent molecule.

At the ONIOM(B3LYP/LANL2DZ:HF/LANL1MB) level, the addition of the second methanol molecule to the joint intermediate **A** leads to an enthalpy gain of 13.4 kcal·mol^{-1} but is found to be just barely exergonic (1.2 kcal·mol^{-1}) because of the entropy loss in the reaction **A**(MeOH) + MeOH → **A**(MeOH)$_2$. In contrast, the second methanol molecule has a dramatic effect on the stability of the C−H transition state, and the enthalpy gain of 21.0 kcal·mol^{-1} is large enough that the addition would be exergonic by 9.0 kcal·mol^{-1}.

At the ONIOM(mPW1K/LANL2DZ+p:mPW1K/LANL2DZ) level, however, we find that **A**(MeOH) + MeOH → **A**(MeOH)$_2$ is endergonic by 5.4 kcal·mol^{-1}. This peculiar result can be ascribed in part to the use of nonoptimum ONIOM(B3LYP/LANL2DZ:HF/LANL1MB) reference geometries, as well as to the use of frequencies and rotational constants at this latter level of theory for the statistical thermodynamics. (The rigid rotor−harmonic oscillator approximation is itself somewhat suspect for systems as nonrigid as those studied here, and complete error cancellation between all species involved cannot be relied upon.) Unfortunately, reoptimization of all structures at the higher level of theory would be beyond our computational resources.

Be that as it may, at all levels of theory we find the barrier from **A**(MeOH)$_2$ to the C−H product to be exceedingly low (2−4 kcal·mol^{-1}), and the rate-determining step for formation of the open-arm C−H product from the closed-arm intermediate **A′** would be the **A**−**A′** interconversion.

Considering the comparable stabilities of the open-arm and closed-arm CH products, as well as the fairly low 9.3 kcal·mol^{-1} C−H activation barrier for the closed-arm system, the two

Table 4. Computed and Observed (X-ray) Values for Selected Geometrical Parameters of the Closed-Arm CC Activation Product without MeOH Ligands[a]

	Distances (Å) and Angles (deg)				
	$\mathbf{P'}_{CC}$ ONIOM(B3LYP/ LANL2DZ: HF/LANL1MB)	$\mathbf{P'}_{CC}$ B3LYP/ LANL2DZ	$\mathbf{P'}_{CC}$ B3LYP/ LANL2dz+p (nonCH)	$\mathbf{P'}_{CC}$-BF_4 B3LYP/ LANL2dz+p (nonCH)	$\mathbf{P'}_{CC}$-BF_4 X-ray structure
Rh−P	2.351	2.379	2.305	2.287	2.2169(4)
Rh−O	2.153	2.145	2.187	2.199	2.1543(13)
Rh−CMe	2.027	2.030	2.028	2.042	2.0220(18)
Rh−CPh	1.974	1.972	1.967	1.979	1.9527(18)
Rh−F				2.286	2.2664(12)
P−Rh−CPh	85.6	85.6	85.8	84.4	83.46(5)
O−Rh−CPh	81.6	81.9	81.3	80.1	81.17(6)
CMe-Rh−CPh	97.1	96.9	97.0	86.8	88.71(8)

[a] Calculated structures are presented both with and without the BF_4^- ligand. The suffix "+p(N,P,O,F)" indicates addition of a d-type polarization function(C_3H_8), and diacetylene (HCCCCH); the methyl radical ($^{\bullet}CH_3$) to B, O, F, and P atoms, and of an f-type polarization function to the metal (see text).

reactions can be regarded as competitive at room temperature, explaining why both closed-arm-and open-arm C−H products are found experimentally. The reverse reaction barriers are significant but still low enough that, upon heating, the thermodynamically favored C−C product can be reached.

Since the methoxy arm is an ether-type ligand, it was of interest to study the effect of an ether solvent on the reaction profile. Very similar results were obtained when we considered the "closed-arm" channel with a single dimethyl ether spectator ligand instead of the methanol molecule.

We finally considered the possibility of adding yet an additional solvent molecule. While we did find local minima for the open-arm $\mathbf{P}_{CH}(MeOH)_3$ and $\mathbf{P}_{CC}(MeOH)_3$ products as well as for the closed-arm $\mathbf{P}_{CC}(MeOH)_2$ product, all of these are endergonic at room temperature. (For the closed-arm $\mathbf{P}_{CH}(MeOH)_2$ product, we could only find a minimum in which the −OMe arm had opened up; this structure exhibits an internal hydrogen bond, the strength of which is expected to be overestimated by more than a factor of 2 because of basis set superposition error.[15]) This structure is found to be exergonic by 5.3 kcal·mol^{-1}, which would probably cease to be the case if larger basis sets were used. Although it was not experimentally observed, we considered a structure of the closed-arm C−H product with three MeOH molecules with the methoxy arm being detached and pointing up. We found a local minimum, but the structure is endergonic at room temperature. The bottom line of these latter "numerical experiments" is that, at room temperature, we can safely rule out structures with more than one coordinated MeOH in the closed-arm case or more than two coordinated MeOH in the open-arm case.

Comparison of Results at Different Levels of Theory. A comparison of relative energies can be found in Table 1. As expected, expanding the basis set from LANL2DZ to LANL2DZ+P reduces the ligand addition energies of the MeOH molecules, because of a reduction in basis set superposition error (BSSE). Some of the relative energies are affected by as much as 10 kcal·mol^{-1} upon addition of polarization functions; the most chemically significant change seen is for the energy difference between the closed-arm (**A′**) and open-arm (**A**) intermediates, which is reduced from −12.2 to −6.2 kcal·mol^{-1} (favoring **A′** in both cases). Working in even larger basis sets (such as the recently proposed SDB-cc-pVTZ basis set[16]) was not possible because of CPU time constraints, but we expect further basis set expansion to affect the energy profile only quantitatively, not qualitatively.

As expected, mPW1K has a tendency to increase barrier heights; it is seen to increase the gap between CC and CH activation barriers compared to B3LYP. Upon comparing the mPW1K/lanl2dz+p and B3LYP/lanl2dz surfaces, perhaps the most striking change seen is the leveling of the path between the two intermediates **A** and **A′**.

Comparison of Computed and X-ray Structures for Closed-Arm CC Product. A comparison of computed and observed structures is given in Table 4. Agreement between the computed ONIOM(B3LYP/LANL2DZ:HF/LANL1MB) and the X-ray structure is rather poor at first sight: large discrepancies exist in particular for the C_{Me}−Rh−C_{ipso} angle (more than 8°) and for the Rh−P distance (0.13 Å). This is not due to the ONIOM approximation: only comparatively minor changes are seen in the computed geometry upon reoptimizing the structure at the B3LYP/LANL2DZ level. A rather drastic change in the Rh−P distance is seen upon introducing polarization functions: in all probability, the remaining gap would be closed-arm if we added additional high-exponent *d* functions to phosphorus.[17] Yet the C_{Me}−Rh−C_{ipso} angle problem noted above remains: it disappears upon introducing the BF_4^- ligand counterion. The latter also causes noticeable changes in the bond distances for the other ligands. Remaining discrepancies between the best computed and the X-ray structures can be ascribed primarily to basis set incompleteness (however, even our rather modest best basis set strained our computational resources to the limit) and secondarily to intrinsic differences between the averaged crystal and bottom-of-the-well gas-phase structures.

Effect of BF_4^- on the Relative Stability of the CC and CH Closed-Arm Products. Given the fairly pronounced effect of the BF_4^- ligand on the closed-arm CC product geometry, we considered the question of whether its coordination, upon evaporation, might affect the relative stability of the closed-arm CC and CH products.

Since fully optimized B3LYP/LANL2DZ+p(hetero) structures are already available for the CC product with and without the BF_4^- ligand, we carried out the corresponding calculations for the CH product as well. The results are somewhat surprising.

At the B3LYP/LANL2DZ+p(hetero) level, without BF_4^-, the CC structure is 8.1 kcal·mol^{-1} more stable than the CH structure. This value does not differ significantly from 8.1 kcal·mol^{-1} at the ONIOM(B3LYP/LANL2DZ:HF/LANL1MB) level, 8.8 kcal·mol^{-1} at the ONIOM(B3LYP/ LANL2DZ+p:B3LYP/ LANL2DZ) level from an ONIOM(B3LYP/LANL2DZ:HF/ LANL1MB) reference geometry, or 5.9 kcal·mol^{-1} at the

(15) E.g.: Evdokimov, A. G.; Kalb (Gilboa), A. J.; Koetzle, T.; Klooster, W.; Martin, J. M. L. *J. Phys. Chem. A* **1999**, *103*, 744.

(16) Martin, J. M. L.; Sundermann, A. *J. Chem. Phys.* **2001**, *114*, 3408.

(17) Martin, J. M. L.; Uzan, O. *Chem. Phys. Lett.* **1998**, *282*, 16.

ONIOM(B3LYP/LANL2DZ+p:B3LYP/LANL2DZ) level from the same reference geometry.

Introducing the additional BF_4^- ligand, however, markedly favors the CC structure over the CH structure. As a result, the $\mathbf{P'}_{CC}$-BF_4 complex ends up being 14.8 kcal·mol^{-1} more stable than the $\mathbf{P'}_{CH}$-BF_4 complex. This marked additional stabilization provides an additional driving force for the formation of the CC product upon solvent evaporation.

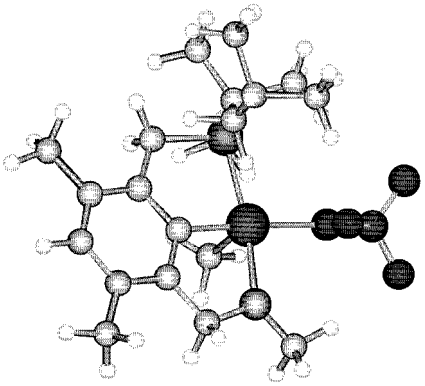

$\mathbf{P'_{CC}–BF_4}$

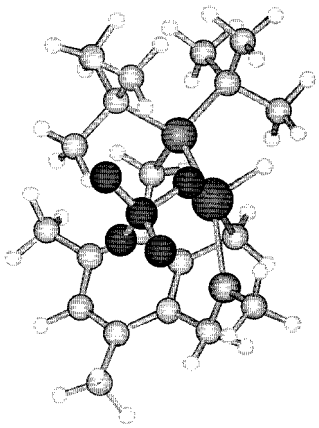

$\mathbf{P'_{CH}–BF_4}$

The better coordination of the BF_4^- anion to the CC ligand is probably best ascribed to steric effects. In the CC case, the complex with BF_4 comfortably achieves a nearly perfect square pyramidal geometry, while in the CH case, the BF_4 ligand has to choose between having the highly electronegative fluorine either cis to the hydride ligand (surely not favorable) or trans to the ligand, and being subject to sterical hindrance from the tertiary butyl groups.

Discussion

Our theoretical calculations reveal the general tendency of the "open-arm" system to prefer C−H over C−C activation, in agreement with the experimental results. It appears that Rh(I) 14e species are significant for both C−C and C−H activation, the calculated barriers being the lowest for the 14e situation. Both thermodynamics and kinetics favor C−H over C−C activation in the "open-arm" PCO case. In the "closed-arm" system our calculations show that C−H activation is kinetically preferred over C−C activation, while the C−C activation product is thermodynamically more stable.

Reactive Intermediates: Aromatic Ring Binding and Agostic Interactions. Theoretical calculations demonstrate that in the case of *neutral* rhodium-PCP systems with bulky substituents (^{i}Pr, ^{t}Bu), the three-coordinate reaction intermediates are stabilized by an agostic interaction with one of the C−H bonds.[8] In the case of less bulky substituents, coordination to the aromatic ring can play a role in the stabilization of the intermediates.[8,18] An analysis of our computational results with regard to the lowest energy reactive intermediates leads to a number of important observations.

(A) The Chelating (Closed-Arm) Case (PCO Ligand with One Bound MeOH Molecule). C−H and C−C bond activation proceed through the common intermediate (Figure 8) with a weak η^1 ring−metal bond, similar to the one found in the case of PCP systems.[8,18] A bond order analysis (Rh−C bond order 0.2) indicates that the stabilizing effect of such a bond is relatively low (the intermediate can be viewed as an essentially 14e species, vide infra). Thus, we suggest that the η^1 binding is a consequence of a rigid bis-chelating structure of the intermediate bringing the metal into close proximity with the aromatic ring and imposing a metal−ring interaction. It can play a role in promoting C−C bond activation since it brings the metal center closer to the C−C bond.[18] However, it does not discriminate significantly between C−H and C−C bonds in the process of activation, as evident from the similar kinetic barriers for both reactions. This weak metal−ring interaction can be viewed as being synergetic with the chelating ligand binding and assisting both C−H and C−C activation.

(B) The Nonchelating (Open-Arm) Case (PCO Ligand with One and Two Bound MeOH Molecules: $\mathbf{A(MeOH)_1}$ and $\mathbf{A(MeOH)_2}$). C−C and C−H bond activation in the open-arm case can start from the intermediate $A(MeOH)_1$, with one MeOH molecule and a genuine η^2 metal−ring interaction or from an intermediate with two methanol molecules $\mathbf{A}(MeOH)_2$, stabilized by an agostic interaction (Figure 8). In the former case, the intermediate can bind an additional molecule of methanol, with concomitant breaking of the metal−ring bond to give a 14e species (vide supra). Although $A(MeOH)_2$ is calculated to be about 5 kcal·mol^{-1} higher in energy than $\mathbf{A}(MeOH)_1$, it may actually be comparable to $A(MeOH)_1$ if solvent effects and larger basis set geometry optimization were applied. In this instance, the lowest energy transition state is reached directly from the corresponding intermediate, simplifying the picture of the reaction profile. In any case, *coordination of two MeOH molecules seems essential to create the lowest energy 14e channel for both C−H and C−C bond activation.*

In both chelating and nonchelating cases, metal−ring interactions seem to be an auxiliary stabilizing factor and can be involved to a minor extent in lowering the activation barrier of C−C activation in the closed-arm case.

Our calculations show that direct bond activation processes are preferable energetically over involvement of C−H agostic species both in the absence and in the presence of the solvent molecules. Yet, local minima on the energy surface can be found for the C−H agostic species, which can also lead to C−C and C−H activation. Since in the case of the agostic intermediates the methoxy arm is detached from the metal, it seems that it is not relevant to C−C bond activation. On the other hand, in the case of C−H activation, one of the intermediates, $\mathbf{A}(MeOH)_2$, was found to be stabilized by an agostic interaction**.** It should be noted that agostic interactions, similar to those found in the PCO open-arm case, were suggested to play an important role in the observed C−H activation/elimination reactivity and selectivity in the PC type complex **5** (which is almost identical to **3a**−**4a**).

(18) Hall, M. B.; Cao, Z. *Organometallics* **2000**, *19*, 3338.

C−H and C−C Bond Activation by a Cationic Rh(I) Complex: Electronic Requirements. C−H bond activation by cationic Rh(I) complexes has not been studied extensively, and computational studies of such systems have not been reported to the best of our knowledge. Computational studies on C−H bond oxidative addition were performed for d^{10} ML_2, d^8 ML_n ($n = 3, 4$; CpML and TpML being special cases), and d^6 ML_n species.[4] In the cases of three- and four-coordinate d^8 RhL_n, which are the most relevant to our studies, it was found that T-shaped 14e intermediates ML_3 are the most reactive in C−H activation. The whole range of RhL_{1-4} intermediates and transition states is possible in the case of the PCO open-arm system. Interestingly, our computational results suggest that the behavior of cationic Rh(I) is essentially comparable to that of its neutral counterpart: 14e intermediates are most active in both the "open-arm" and "closed-arm" systems. The fact that the metal center coordinates solvent molecules in order to achieve the 14e configuration demonstrates the general importance of this electronic structure for the C−H bond activation. Importantly, relatively poor electron donating ligands such as methanol molecules are sufficient to provide the electron density necessary for C−H bond activation, most probably due to the cationic nature of the metal center, which can coordinate the hard solvent molecules better than a neutral center. It appears that the electron density of the $[R_3PRh(MeOH)_2]^+$ fragment, which is probably lower compared to most of the known examples of d^8 intermediates in C−H activation, is adequate for the C−H activation process.

Significantly, the same electronic requirements are necessary for C−C bond activation. Our computational results show that 14e intermediates are involved in the lowest energy pathways for C−C bond oxidative addition.

Sterics of C−C vs C−H Bond Activation: Comparison of Transition States. According to the computational results, both C−C and C−H bond oxidative addition in the PCO−Rh system proceed through three-centered transition states, similar to the neutral PCP and PCN systems.

A comparison of the transition states for C−C and C−H bond activation (Figure 9) reveals a striking difference between the open-arm and closed-arm cases. Whereas in the closed-arm system the transition states for both C−C and C−H activation have similar geometries (**TS-A′P′**$_{CC}$ and **TS-A′P′**$_{CH}$), in the open-arm case their geometries differ significantly (**TS-AP**$_{CC}$ and **TS-AP**$_{CH}$). In **TS-A′P′**$_{CC}$ and **TS-A′P′**$_{CH}$, the metal center is situated in close proximity to both the C−H and C−C bonds, which is reflected in similar barriers of activation. C−H activation in the open-arm case proceeds through **TS-AP**$_{CC}$, in which a metal center is not situated in close proximity to the C−C bond. For the C−C bond to be cleaved (**TS-AP**$_{CH}$), the metal must approach it in a mode similar to the closed-arm system, where it is already held in a proximal position. Thus, in terms of the reaction kinetics, the outer bond, C−H, is more available for activation, while the inner C−C can stay intact in the open-arm system. Since C−C activation in the open-arm system is disfavored thermodynamically as well, the C−H product is the only possible one in the open-arm system. In the closed-arm case, chelation results in a geometry which favors both C−C and C−H oxidative addition, due to the proximity of the metal to these bonds. It should be noted that the experimental ratio of the closed-arm and open-arm C−H activation products in methanol and the calculated kinetic barriers suggest that there is no significant preference for C−H activation in the closed-arm case as compared with the open-arm one. On the other hand, C−C bond activation is unfavorable in the nonchelating case. This reflects the significance of the specific steric requirements for C−C bond activation, which can be imposed by chelation.

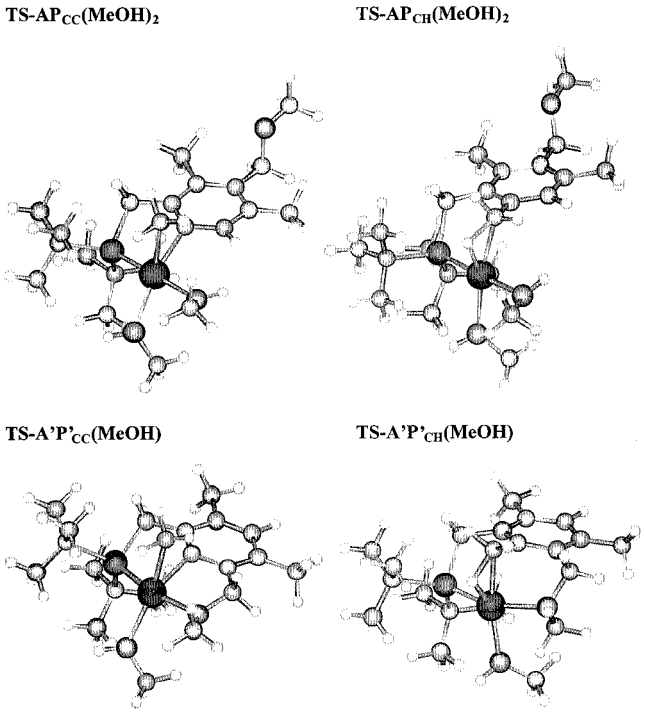

Figure 9. Perspective view of selected structures of selected transition states.

Although the open-arm system favors C−H activation both kinetically and thermodynamically, the relatively small difference in the stability of the C−H and C−C products and the reasonable kinetic barrier required for C−C bond activation suggest that the C−H vs C−C reaction aptitudes can be reversed by an appropriate system design. Relevant studies are currently under way in our group.

Conclusions

We have demonstrated both carbon−hydrogen and carbon−carbon bond activation in a novel PCO ligand system. The importance of the chelate effect for C−C bond cleavage was clearly demonstrated. The computational study of the system provides important insights into the reaction mechanism. Theoretical calculations demonstrate that the steric requirements for C−C bond activation are more restricting than for the C−H one, and therefore chelation is much more important for the cleavage of the C−C bond. On the other hand, the electronic requirements for both C−C and C−H are very similar, and 14e intermediates play a key role in both activation processes. We also note that coordinating solvent molecules significantly affect the reaction profiles, and much more so for the open-arm than for the closed-arm system.

Notably, in an unprecedented observation, conversion of a C−H activated product complex into a C−C activated one was achieved solely by solvent evaporation. Theoretical calculations suggest that this is largely due to the special effect of BF_4^- coordination upon solvent evaporation.

Experimental Methods

All experiments with metal complexes and the phosphine ligand were carried out under an atmosphere of purified nitrogen in an MBraun MB 150B-G glovebox. The complex $[Rh(coe)_2Cl]_2$ was prepared according to a literature procedure.[19]

^{1}H, ^{13}C, and ^{31}P NMR spectra were recorded at 400, 100, and 162 MHz, respectively, at 295 K, using a Bruker Avance-400 NMR spectrometer. ^{1}H NMR and ^{13}C{^{1}H} NMR chemical shifts are reported in ppm downfield from tetramethylsilane. ^{1}H NMR chemical shifts are referenced to the residual hydrogen signal of the deuterated solvents, and in ^{13}C{^{1}H} NMR the ^{13}C signal of the deuterated solvents was used as a reference. ^{31}P NMR chemical shifts are reported in ppm downfield from H_3PO_4 and referenced to an external 85% solution of phosphoric acid in D_2O. Abbreviations used in the description of NMR data are as follows: Ar, aryl; br, broad; dist, distorted; s, singlet; d, doublet; m, multiplet. Electrospray (ES) mass spectrometry was performed using a MicroMass LCZ Detector 4000 with CV = 43 V, temperature = 150 °C, and EE = 4.2 V. Elemental analysis was performed at the Hebrew University of Jerusalem.

Synthesis of $C_6H(CH_3)_3(CH_2OCH_3)(CH_2Br)$. A freshly prepared methanol solution of NaOMe (0.53 g, 9.81 mmol) was added dropwise to a THF solution of 1,3-bis(bromomethyl)-2,4,6-trimethylbenzene[11] (3.00 g, 9.81 mmol) at 0 °C. The solution was stirred for 2 h at room temperature, and the solvent was evaporated under vacuum. This yielded the monomethoxy compound, 1-bromomethyl-3-methoxymethyl-2,4,6-trimethylbenzene, which was purified by column chromatography (SiO_2, hexane:THF) to give 1.34 g (53.3% yield) of the pure product as a white solid.

^{1}H NMR ($CDCl_3$): 6.87 (s, 1H, Ar-*H*), 4.57 (s, 2H, Ar−CH_2−Br), 4.44 (s, 2H, Ar−CH_2−O), 3.39 (s, 3H, O−CH_3), 2.41 (s, 3H, Ar−CH_3), 2.35 (s, 3H, Ar−CH_3), 2.34 (s, 3H, Ar−CH_3).

Synthesis of $C_6H(CH_3)_3(CH_2OCH_3)(CH_2P(t\text{-}Bu)_2)$ (1). HP(t-Bu)$_2$ (0.890 g, 6.09 mmol) was added to a solution of $C_6H(CH_3)_3(CH_2OCH_3)(CH_2Br)$ (1.30 g, 5.06 mmol) in acetone. The resulting solution was refluxed for 30 min, followed by solvent evaporation under vacuum. The residue was washed with ether, and the resulting phosphonium salt was dissolved in degassed water, treated with NaOAc, and extracted with ether. Final purification of the phosphine **1** was accomplished by column chromatography (SiO_2, hexane:THF) to afford 1.14 g (70% yield) of the PCO ligand **1**, 1-methoxymethyl-3-(di-*tert*-butylphosphino)methyl-2,4,6-trimethylbenzene, as a colorless oil.

^{31}P{^{1}H} NMR (benzene-d_6): 26.38 (s). ^{1}H NMR (benzene-d_6): 6.80 (s, 1H, Ar-*H*), 4.35 (s, 2H, Ar−CH_2−O), 3.15 (s, 3H, O−CH_3), 2.81 (d, $^2J_{PH}$ = 2.0 Hz, 2H, Ar−CH_2−P), 2.65 (s, 3H, Ar−CH_3), 2.47 (s, 3H, Ar−CH_3), 2.27 (s, 3H, Ar−CH_3), 1.08 (d, $^3J_{PH}$ = 10.3 Hz, 18H, 2 P−C(CH_3)$_3$). ^{13}C{^{1}H} NMR (benzene-d_6): 137.05 (s, Ar), 136.07 (s, Ar), 136.05 (d, J_{PC} = 11.0 Hz, Ar), 134.76 (s, Ar), 133.34 (s, Ar), 130.8 (d, J_{PC} = 9.0 Hz, Ar), 69.46 (s, Ar−*C*H_2−O), 57.45 (dd, J = 10.3 Hz, J = 4.6 Hz, O−*C*H_3), 32.32 (d, $^1J_{PC}$ = 26.2 Hz, 2 P−*C*(CH$_3$)$_3$), 29.95 (d, $^2J_{PC}$ = 13.0 Hz, 2 P−C(*C*H$_3$)$_3$), 24.17 (d, $^1J_{PC}$ = 29.7 Hz, Ar−*C*H_2−P), 22.31 (d, J = 8.4 Hz, Ar−*C*H_3), 19.77 (d, J = 6.1 Hz, Ar−*C*H_3), 17.73 (br s, Ar−*C*H_3). ^{1}H and ^{13}C{^{1}H} NMR signal assignment was confirmed by ^{13}C−^{1}H correlation and ^{13}C DEPT.

Reaction of $[Rh(coe)_2(solv)_n]BF_4$ with the PCO Ligand 1. Formation of C−H Activation Products 2−4. A THF (3 mL) solution of $AgBF_4$ (12 mg, 0.062 mmol) was added to a THF solution (4 mL) of $[Rh(coe)_2Cl]_2$ (22 mg, 0.031 mmol). Immediate precipitation of AgCl took place, and the precipitate was removed by filtration after the mixture was allowed to stand at room temperature for 15 min. The resulting clear orange solution was evaporated under vacuum to yield $[Rh(coe)_2(solv)_n]BF_4$. This was then redissolved in THF, methanol, or acetone to yield an orange solution in every solvent. To each of these solutions was added a solution of 20 mg (0.062 mmol) of the PCO ligand in the corresponding solvent. The color of the THF solution changed to brown after a few minutes, whereas in methanol or acetone there was no noticeable color change. The solution was kept at room temperature for 1 h, resulting in formation of the C−H activation products **3** and **4**. Complex **2** was not sufficiently stable for spectroscopic characterization. Complexes **3** (in acetone) and **4** (in methanol) exist in solution as a mixture of open-arm (**3a**, **4a**) and closed-arm (**3b**, **4b**) forms. In the closed-arm form, the methoxy sidearm is coordinated to the rhodium center. In the open-arm form this arm is not coordinated and is replaced by a solvent molecule.

Complex 3 (3a:3b = 1:4.4). ^{31}P{^{1}H} NMR (acetone-d_6): 130.4 (d, $^1J_{RhP}$ = 192.2 Hz, **3b**), 126.5 (d, $^1J_{RhP}$ = 191.5 Hz, **3a**). ^{1}H NMR (acetone-d_6, only selected signals of **3a** (minor product) are given, integration is given only for **3b** (major product)): 6.88 (s, Ar−*H*, **3a**), 6.77 (s, 1H, Ar−*H*, **3b**), 4.97 (d, $^2J_{HH}$ = 12.5 Hz, 1H, Ar−CH_2−O, left part of AB-system, **3b**), 4.61 (d, $^2J_{HH}$ = 12.7 Hz, 1H, Ar−CH_2−O, right part of AB-system, **3b**), 4.38 (s, Ar−CH_2−O, **3a**), 3.27 (s, 3H, O−CH_3, **3b**), 3.06 (dd, $^2J_{HH}$ = 8.8 Hz, $^2J_{PH}$ = 3.7 Hz, 1H, Ar−CH_2−P, left part of AB-system, **3b**), 2.59 (br m, 4H, overlapping signals of Ar−CH_2−P and Ar−CH_2−Rh, **3b**), 2.42 (s, Ar−CH_3, **3a**), 2.36 (s, 3H, Ar−CH_3, **3b**), 2.34 (s, 3H, Ar−CH_3, **3b**), 2.28 (s, Ar−CH_3, **3a**), 1.62 (d, $^3J_{PH}$ = 12.5 Hz, 9H, P−C(CH_3)$_3$, **3b**), 1.48 (br s, P−C(CH_3)$_3$ of **3b**), 1.07 (d, $^3J_{PH}$ = 13.1 Hz, 9H, P−C(CH_3)$_3$, **3b**), −24.70 (br m, Rh−H, **3a**), −24.89 (dd, $^1J_{RhH}$ = 27.2 Hz, $^2J_{PH}$ = 18.1 Hz, 1H, Rh-*H*, **3b**). Selected ^{13}C{^{1}H} NMR (acetone-d_6): 8.85 (d, $^1J_{RhC}$ = 25.1 Hz, Ar−*C*H_2−Rh, **3b**).

Complex 4 (4a:4b = 1.5:1). ^{31}P{^{1}H} NMR (methanol-d_4): 126.8 (d, $^1J_{RhP}$ = 195.8 Hz, **4b**), 126.3 (d, $^1J_{RhP}$ = 194.8 Hz, **4a**). ^{1}H NMR (methanol-d_4, integration relates to **4a** and **4b** separately): 6.95 (s, 1H, Ar−*H*, **4b**), 6.76 (s, 1H, Ar−*H*, **4a**), 4.61 (s, 2H, Ar−CH_2−O, **4a**), 4.44 (dd, J = 9.1 Hz, J = 9.0 Hz, 2H, Ar−CH_2−O, **4b**), 3.46 (s, 3H, O−CH_3, **4a**), 3.34 (d, J = 3.1 Hz, 3H, O−CH_3, **4a**), 2.83 (m, 2H, Ar−CH_2−Rh, **4b**), 2.75 (m, 2H, Ar−CH_2−Rh, **4a**), 2.46 (s, 3H, Ar−CH_3, **4b**), 2.42 (s, 3H, Ar−CH_3, **4b**), 2.37 (s, 3H, Ar−CH_3, **4b**), 2.32 (s, 3H, Ar−CH_3, **4a**), 2.31 (s, 3H, Ar−CH_3, **4a**), 2.29 (s, 3H, Ar−CH_3, **4a**), 1.43 (d, $^3J_{PH}$ = 12.5 Hz, 9H, P−C(CH_3)$_3$, **4b**), 1.35 (d, $^3J_{PH}$ = 12.5 Hz, 9H, P−C(CH_3)$_3$, **4a**), 1.17 (d, $^3J_{PH}$ = 12.5 Hz, 9H, P−C(CH_3)$_3$, **4b**), 1.23 (d, $^3J_{PH}$ = 13.1 Hz, 9H, P−C(CH_3)$_3$, **4a**), −25.28 (dd, $^1J_{RhH}$ = 27.4 Hz, $^2J_{PH}$ = 21.2 Hz, 1H, Rh−H, **4a**), −25.49 (dd, $^1J_{RhH}$ = 28.0 Hz, $^2J_{PH}$ = 20.9 Hz, 1H, Rh-*H*, **4b**). ES-MS (methanol solution): M^+ found 425.31, calcd for $C_{20}H_{35}OPRh$ 425.37 (no solvent molecules or BF_4 are present); M^- found 86.95, calcd for BF_4 86.8.

Reaction of the C−H Activation Products 2−4 with Ethylene Glycol. Ethylene glycol was added in a large excess (10 equiv) to a solution of complexes **2**−**4** in THF, methanol, or acetone. The solution was left at room temperature for 1 h, and then the solvent was evaporated under vacuum. The resulting residue was washed with pentane and ether to remove excess of ethylene glycol and dried under vacuum.

^{31}P{^{1}H} NMR (methanol-d_4): 127.1 (dd, $^1J_{RhP}$ = 193.5 Hz), 126.7 (dd, $^1J_{RhP}$ = 194.2 Hz). Selected ^{1}H NMR signals (methanol-d_4): 6.95 (s, 1H, Ar-*H*), 6.75 (s, 1H, Ar−*H*), 4.84 (s, 2H, Ar−CH_2−O), 4.62 (s, 2H, Ar−CH_2−O), 4.42 (d, J = 1.6 Hz, 2H, Ar−CH_2−O), 3.64 (s, 4H, O−CH_2CH_2−O), 3.45 (s, 3H, O−CH_3), 3.35 (s, 3H, O−CH_3), −25.2 (dd, $^1J_{RhH}$ = 39.2 Hz, $^2J_{PH}$ = 27.6 Hz, Rh−*H*), −25.2 (d, $^2J_{PH}$ = 27.1 Hz, Rh−*H*).

Formation of the C−C Activation Product 6. (a) Solutions of complexes **2**−**4** in THF, methanol, or acetone were dried under vacuum at room temperature for 3 days and redissolved in methanol to form the C−C activation product **6** (70−80% yield). (b) Heating of a methanol solution of **4** at 70 °C for 1 h leads to formation of **6** in 85% yield (^{31}P{^{1}H}-NMR). Further heating leads to significant decomposition. Heating in acetone or THF also results in formation of C−C activation products, but the reactions are not clean enough to characterize the products.

^{31}P{^{1}H} NMR (methanol-d_4): 90.2 (d, $^1J_{RhP}$ = 190.8 Hz). ^{1}H NMR (methanol-d_4): 6.55 (s, 1H, Ar−*H*), 5.13 (d, $^2J_{HH}$ = 12.9 Hz, 1H, Ar−CH_2−O, left part of AB-system), 5.00 (d, $^2J_{HH}$ = 12.8 Hz, 1H, Ar−CH_2−O, right part of AB-system), 4.88 (s, 3H, O−CH_3), 3.82 (br d, $^2J_{PH}$ = 1.1 Hz, 2H, Ar−CH_2−P), 2.25 (s, 3H, Ar−CH_3), 2.11 (s, 3H, Ar−CH_3), 1.38 (d, $^3J_{PH}$ = 13.5 Hz, 9H, P−C(CH_3)$_3$), 1.22 (d, $^3J_{PH}$ = 12.8 Hz, 9H, P−C(CH_3)$_3$), 1.02 (d, $^2J_{RhH}$ = 2.3 Hz, 3H, Rh−CH_3). ^{13}C{^{1}H} NMR (methanol-d_4): 157.02 (dd, $^1J_{RhC}$ = 35.7 Hz, $^2J_{PC}$ = 4.7 Hz, ipso C_{Ar}−Rh), 144.50 (dd, ^2J = 8.3 Hz, ^2J = 3.5 Hz, Ar), 140.25 (s, Ar), 133.21 (d, $^2J_{RhC}$ = 15.9 Hz, Ar), 130.06 (s, Ar), 128.19 (s, Ar), 82.52 (s, Ar−*C*H_2−O), 68.83 (s, O−*C*H_3), 38.77 (d, $^1J_{PC}$ = 21.9 Hz, P−*C*(CH$_3$)$_3$), 36.92 (dd, $^1J_{PC}$ = 19.5 Hz, $^2J_{RhC}$ = 2.8 Hz, P−*C*(CH$_3$)$_3$), 31.68 (dd, $^1J_{PC}$ = 31.0 Hz, $^2J_{RhC}$ = 3.9 Hz, Ar−*C*H_2−P), 31.07 (d, $^2J_{PC}$ = 2.5 Hz, P−C(*C*H$_3$)$_3$), 29.74 (d, $^2J_{PC}$ = 2.1 Hz, P−C(*C*H$_3$)$_3$), 20.94 (s, Ar−*C*H_3), 19.16 (s, Ar−*C*H_3), −4.55 (dd, $^1J_{RhC}$ = 32.0 Hz, $^2J_{PC}$ = 8.3 Hz, Rh−*C*H_3). ES-MS (methanol solution): *m*/*e* 425.37, M^+ calcd for $C_{20}H_{35}OPRh$ 425.37 (no solvent molecules are present). ES-MS: M^- found 86.96, calcd for BF_4 86.80.

Elemental Analysis (after prolonged evaporation). Calcd for $C_{20}H_{35}BF_4OPRh$ (no solvent molecules present): C, 46.90; H, 6.89. Found: C, 47.73; H, 7.81.

(19) Herde, J. L.; Senoff, C. V. *Inorg. Nucl. Chem. Lett.* **1971**, *7*, 1029.

X-ray Structural Analysis of Complex 6. Complex **6** was crystallized by dissolving the solid in boiling diethyl ether, followed by cooling the solution to room temperature. Allowing the ether solution to stand at room temperature overnight yielded orange prismatic crystals.

Crystal Data: $C_{20}H_{35}OPRh + BF_4$, orange prisms, $0.3 \times 0.2 \times 0.2$ mm^3, monoclinic, $P2_1/c$ (No. 14), $a = 13.8280(3)$ Å, $b = 11.8580(3)$ Å, $c = 15.0660(4)$ Å, $\beta = 114.7050(15)°$, from 10° of data, $T = 120$ K, $V = 2211.84(9)$ Å^3, $Z = 4$, fw = 512.17, $D_c = 1.538$ Mg/m^3, $\mu = 0.886$ mm^{-1}.

Data Collection and Treatment: Nonius KappaCCD diffractometer, MoKα ($\lambda = 0.71073$ Å), graphite monochromator, 17 604 reflections collected, $0 < h \leq 18$, $0 \leq k \leq 16$, $-20 \leq l \leq 18$, frame scan width = 2.0°, scan speed 1° per 20 s, typical peak mosaicity = 0.6°, 5630 independent reflections ($R_{int} = 0.028$). Data were processed with Denzo-Scalepack.

Solution and Refinement. The structure was solved by direct methods with SHELXS-97, followed by full matrix least-squares refinement based on F^2 with SHELXL-97 (279 parameters with no restraints). Idealized hydrogens were placed and refined in a riding mode. The final R-factors are $R_1 = 0.025$ (based on F^2) for data with $I > 2\sigma(I)$, and $R_1 = 0.030$ on all 5630 reflections. The goodness-of-fit on F^2 is 1.046, and the largest electron density equals 1.011 e/Å^3.

Computational Methods

All calculations were carried out using the Gaussian 98 program system[20] running on Compaq ES40 and XP1000 computers in our research group, as well as on the (Israel) Inter-University Computing Center (IUCC) SGI Origin 2000.

As in our previous studies on the PCP[8] and PCN[21] systems, the initial survey of the potential surface was carried out by a two-layer ONIOM[22] approach, in which only the *tert*-butyl groups on the phosphorus were placed in the outer layer, and the remainder of the system was placed in the inner layer. The inner layer was treated using the B3LYP[23] exchange-correlation functional with the Los Alamos National Laboratory double-ζ (LANL2DZ) basis set−relativistic effective core potential (RECP) combination.[24] (As is customary, first-row atoms in this approach were treated by means of the Dunning−Hay valence double-ζ[25] basis set.) The *tert*-butyl substituents in the outer layer were treated at the Hartree−Fock level with the LANL1MB basis set−RECP combination.[24]

Geometry optimizations for minima were carried out using the standard Schlegel algorithm[26] in redundant internal coordinates until in the neighborhood of the solution and then continued using analytical second derivatives.[27] Optimizations for transition states were carried out by means of the QST3 approach,[28] with an initial guess for the transition state being generated from either linear synchronous transit (LST[29]) or from manual manipulation of the geometry using MOLDEN.[30] In cases where this approach failed to converge, we likewise used analytical second derivatives at every step.

Where necessary, the Grid = UltraFine combination, i.e., a pruned (99 590) grid in the integration and gradient steps and a pruned (50 194) grid in the CPKS (coupled perturbed Kohn−Sham) steps, was used as recommended in ref 31. While an overly coarse grid convergence obviously cannot cause false symmetry breaking here (of the sort previously noted for the PCP system[8]), we did encounter a number of cases for which no structure with all real frequencies could be obtained unless we switched to the "ultrafine" grid combination.

Zero-point and RRHO (rigid rotor−harmonic oscillator) thermal corrections were obtained from the unscaled computed frequencies.

Where necessary to resolve ambiguities about the nature of a transition state, intrinsic reaction coordinate (IRC[32]) calculations were carried out.

The energetics for our final profile were validated by single-point energy calculations, using the ONIOM(B3LYP/LANL2DZ:HF/LANL1MB) reference geometries, at two higher levels of theory. The first is ONIOM(B3LYP/LANL2DZ+P:B3LYP/LANL2DZ), where the "+P" stands for the addition of polarization functions with exponents taken from ref 33. The second is ONIOM(mPW1K/LANL2DZ+P:mPW1K/LANL2DZ), in which the very recent mPW1K (modified[34] Perdew−Wang 1991[35] for Kinetics) exchange-correlation functional of Truhlar and co-workers[36] was employed. This functional was very recently shown[37] to yield more reliable reaction barrier heights than other exchange-correlation functionals.

To assist with interpretation, natural bond orbital (NBO) analyses[38] with Wiberg bond orders[39] were carried out.

Acknowledgment. D.M. is the Israel Matz Professor of Organic Chemistry and J.M.L.M. the incumbent of the Helen and Milton A. Kimmelman Career Development Chair. S.O. acknowledges a postdoctoral fellowship from the Minerva Foundation, Munich, Germany. This research was supported by the *Tashtiyot* program of the Ministry of Science (Israel), by the Israel Science Foundation, and by the US-Israel Binational Science Foundation, Jerusalem, Israel. We gratefully acknowledge support from the Helen and Martin Kimmel Center for Molecular Design.

Supporting Information Available: Cartesian coordinates for all computed ONIOM(B3LYP:LANL2DZ:HF/LANL1B) structures in XMol (.xyz) format; total energies of all computed structures; crystallographic data in plain text and CIF (Crystallographic Information File) format; and B3LYP/LANL2DZ electron density plots (color GIF format) of **A**(MeOH), **TS-AP**$_{CH}$MeOH, **TS-AP**$_{CH}$(MeOH)$_2$, **TS-A′P′**$_{CC}$(MeOH), and **TS-A′P′**$_{CH}$(MeOH) are available on the World Wide Web at http://theochem.weizmann.ac.il/web/papers/pco.html. This material is also available free of charge via the Internet at http://pubs.acs.org.

JA016126T

(20) Frisch, M. J.; Trucks, G. W.; Schlegel, H. B.; Scuseria, G. E.; Robb, M. A.; Cheeseman, J. R.; Zakrzewski, V. G.; Montgomery, J. A.; Stratmann, R. E.; Burant, J. C.; Dapprich, S.; Millam, J. M.; Daniels, A. D.; Kudin, K. N.; Strain, M. C.; Farkas, O.; Tomasi, J.; Barone, V.; Cossi, M.; Cammi, R.; Mennucci, B.; Pomelli, C.; Adamo, C.; Clifford, S.; Ochterski, J.; Petersson, G. A.; Ayala, P. Y.; Cui, Q.; Morokuma, K.; Malick, D. K.; Rabuck, A. D.; Raghavachari, K.; Foresman, J. B.; Cioslowski, J.; Ortiz, J. V.; Stefanov, B. B.; Liu, G.; Liashenko, A.; Piskorz, P.; Komaromi, I.; Gomperts, R.; Martin, R. L.; Fox, D. J.; Keith, T.; Al-Laham, M. A.; Peng, C. Y.; Nanayakkara, A.; Gonzalez, C.; Challacombe, M.; Gill, P. M. W.; Johnson, B. G.; Chen, W.; Wong, M. W.; Andres, J. L.; Head-Gordon, M.; Replogle, E. S.; Pople, J. A.; *Gaussian 98*, Revision A.7; Gaussian, Inc.: Pittsburgh, PA, 1998.

(21) Sundermann, A.; Uzan, O.; Martin, J. M. L. *Organometallics* **2001**, *20*, 1783.

(22) Dapprich, S.; Komaromi, I.; Byun, K. S.; Morokuma, K.; Frisch, M. J. *J. Mol. Struct. (THEOCHEM)* **1999**, *461*, 1 and references therein.

(23) Becke, A. D. *J. Chem. Phys.* **1993**, 98, 5648. Lee, C.; Yang, W.; Parr, R. G. *Phys. Rev. B* **1988**, *37*, 785.

(24) Hay, P. J.; Wadt, W. R. *J. Chem. Phys.* **1985**, *82*, 270, 284, 299.

(25) Dunning, T. H.,; Hay, P. J. In *Modern Theoretical Chemistry*; Schaefer, H. F., III, Ed.; Plenum: New York, 1976; Vol. 3.

(26) Schlegel, H. B. *J. Comput. Chem.* **1982**, *3*, 214. Peng, C.; Ayala, P. Y.; Schlegel, H. B.; Frisch, M. J. *J. Comput. Chem.* **1996**, *17*, 49.

(27) Stratmann R. E.; Burant J. C.; Scuseria G. E.; Frisch M. J. *J. Chem. Phys.* **1997**, *106*, 10175.

(28) Peng, C.; Schlegel, H. B. *Isr. J. Chem.* **1994**, *33*, 449.

(29) Halgren, T. A.; Lipscomb, W. N. *Chem. Phys. Lett.* **1977**, *49*, 225.

(30) Schaftenaar, G. Molden 3.6, 1999. URL: http://www.cmbi.kun.nl/~schaft/molden/molden.html.

(31) Martin, J. M. L.; Bauschlicher, C. W., Jr.; Ricca, A. *Comput. Phys. Commun.* **2001**, *133*, 189.

(32) Gonzalez, C.; Schlegel, H. B. *J. Chem. Phys.* **1989**, *90*, 2154; *J. Phys. Chem.* **1990**, *94*, 5523.

(33) Hollwarth, A.; Bohme, M.; Dapprich, S.; Ehlers, A. W.; Gobbi, A.; Jonas, V.; Kohler, K. F.; Stegmann, R.; Veldkamp, A.; Frenking, G. *Chem. Phys. Lett.* **1993**, *208*, 237. Ehlers, A. W.; Bohme, M.; Dapprich, S.; Gobbi, A.; Hollwarth, A.; Jonas, V.; Kohler, K. F.; Stegmann, R.; Veldkamp, A.; Frenking, G. *Chem. Phys. Lett.* **1993**, *208*, 111.

(34) Adamo, C.; Barone, V. *J. Chem. Phys.* **1998**, *108*, 664.

(35) Perdew, J. P.; Chevary, J. A.; Vosko, S. H.; Jackson, K. A.; Pederson, M. R.; Singh, D. J.; Fiolhais, C. *Phys. Rev. B* **1992**, *46*, 6671 and references therein.

(36) Lynch, B. J.; Fast, P. L.; Harris, M.; Truhlar, D. G. *J. Phys. Chem. A* **2000**, *104*, 4811.

(37) Parthiban, S.; de Oliveira, G.; Martin, J. M. L. *J. Phys. Chem. A.* **2001**, *105*, 895. Lynch, B. J.; Truhlar, D. G. *J. Phys. Chem. A* **2001**, *105*, 2936.

(38) Reed, A. E.; Curtiss, L. A.; Weinhold, F. *Chem. Rev.* **1988**, *88*, 899.

(39) Wiberg, K. B. *Tetrahedron* **1968**, *24*, 1083.